RADIATIVE TRANSFER IN THE MIDDLE ATMOSPHERE AND PLANETARY ATMOSPHERES

XUN ZHU

The Johns Hopkins University Applied Physics Laboratory
11100 Johns Hopkins Road, Laurel, MD 20723-6099, USA
E-mail: xun.zhu@jhuapl.edu

Radiative heat exchange is the major energy source in the Earth's middle atmosphere and most models of planetary atmospheres. In this article, the author will start with the basic radiative transfer equation and its formal solution from the perspective of radiative heating and cooling rate calculations in numerical models for the middle atmosphere and planetary atmospheres. The exposition of the radiative transfer theory will be presented along three major lines that lead to the goal of heating and cooling rate calculations in a clear-sky atmosphere. First, the basic quantum concepts of the microscopic interactions between photons and particles and the physical mechanisms of absorption and emission line profiles will be summarized. Second, the traditional approaches of band models associated with frequency integration will be briefly reviewed with a special emphasis on the recently developed correlated-*k* distribution method. Third, the physical nature of the source function associated with non-local thermodynamic equilibrium processes will be discussed. Finally, a few selected applications of radiative transfer theory in the middle atmosphere and planetary atmospheres will be presented in the context of how the objective of high accuracy and efficiency is accomplished while solving various types of radiative transfer problems.

1. Introduction

It is often said that solar radiation is the ultimate source of energy for atmospheric and oceanic circulations because the Earth has no significant internal source of its own energy. However, to understand the physical basis of atmospheric and oceanic circulations and their variabilities, one must understand the direct energy or momentum sources that drive the circulations. For example, many of the observed characteristics of large-scale oceanic circulations can be entirely attributed to forcing by the surface wind stress (e.g., Pedlosky 1987, Ch. 5). Three well-known types of energy that drive the atmospheric circulation are net radiative heating, sensible heating, and latent heating. Calculations of the energy budget in the atmosphere on these three types of energy show comparable contributions from all the sources (Peixoto and Oort 1992, p. 366). Since the troposphere consists of 90% of the whole atmosphere, the energy budget reflects mainly the atmospheric structure in the troposphere.

Sensible and latent heat sources mostly result from the unstable convection and the formation or dissipation of clouds. However, few clouds exist in the Earth's middle atmosphere (altitude: $z \sim$ 10-100 km) due to its relatively stable vertical stratification. Hence we expect that radiative heat exchange is the dominant energy source in the middle atmosphere. Furthermore, because of the scarcity of clouds in the middle atmosphere, radiative transfer can be studied without considering multiple scattering processes. Emission and absorption take place in the middle atmosphere under "clear-sky" conditions, where the absorbers' radiation properties are slowly varying with time and space. As a result, the net radiative heating rate (H_{r_net}) is often the most accurately evaluated forcing term in middle

atmosphere models. Since the contributions from the sensible and latent heating are negligibly small in magnitude with greater uncertainties H_{r_net} is the only thermal forcing term in many middle atmosphere models.

Professor Jijia Zhang taught many of the authors in this collection of papers a course "Atmospheric General Circulations" at Nanjing Institute of Meteorology in the early 1980s. Part of the lecture notes (Zhang 1981) introduced a simple radiative transfer theory of a gray atmosphere in which the theory of the vertical thermal structure of the Earth's atmosphere was developed following the historical works by Emden (1913), Kibel (1943), etc. The modern theory of radiative transfer has introduced many fundamental advances in the understanding of the physical nature of the emission/absorption processes and in techniques for calculating radiative heat exchange in the atmosphere (e.g., Goody and Yung 1989). However, the basic ideas of radiative heat exchange, energy balance, radiative-convective adjustment, etc., embedded in those lectures remain valid and also inspired us to pursue our careers in different fields of atmospheric sciences. Furthermore, some studies in the planetary atmospheres are following a path similar to that of the early history of meteorology due to a similar situation of having only limited sets of observations.

In this article, the ideas and techniques of middle atmosphere radiative transfer theory and its applications will be explored in an informal and hierarchical style from which readers with different backgrounds could all benefit. This article is tutorial in nature, and most of the material can serve as an introduction to the field. It also contains a brief review on the recent developments in the field and several expository views by the author from different perspectives. Section 2 gives a descriptive introduction to the basic quantum concept of discrete energy levels and some consequences in applying the idea to atmospheric radiation. Section 3 establishes the macroscopic radiative transfer equation (RTE) and its formal solution for heating and cooling rate calculations. The basic ideas of two remote sounding techniques (occultation and limb emission-absorption) together with their pros and cons are also briefly described based on the formal solution of the RTE. Section 4 briefly shows how the atmospheric spectra are formed. Section 5 reviews the two most widely used tools in the integration of radiance over frequency. Section 6 establishes the microscopic RTE and its relation to the macroscopic one. The rate equation and a few simple solutions to the source function are also described. Readers who are newcomers to the field of atmospheric radiation or who are interested only in stratospheric radiation theory may skip this section. Section 7 presents several applications of the radiative transfer theory to planetary atmospheres and the Earth's middle atmosphere, based on author's own research experience. Special emphasis is placed on how to reach an appropriate balance between accuracy and efficiency for different types of problems. Finally, Section 8 provides concluding remarks and additional references.

2. The Basic Quantum Concepts of Interaction Between Radiation and Matter

In the late 1800s, physicists were convinced that light, heat radiation, and radio waves were all electromagnetic waves differing only in frequency and wavelength. However, the spectral distribution of radiation from a heated cavity could not be explained by classical (Maxwell) wave theory. Max Planck's solution to the problem was to introduce the new concept that radiation could only take discrete or quantized energies (joule = kg m^2 s^{-2}) given by

$$E_{light} = nh\nu, \tag{1}$$

where n is an integer, h ($= 6.626 \times 10^{-34}$ J s) is the Planck constant, and ν (s^{-1}) is the wave frequency. Therefore, light consists of a stream of discrete photons. A photon can be thought of as a wave packet that carries an electromagnetic field of energy $E = h\nu$. For example, each photon emitted by a radio station of frequency, say, 630 kHz ($= 6.3 \times 10^5$ s^{-1}) carries 4.17×10^{-28} joules of energy. Each photon emitted from a red traffic light ($\nu \approx 4 \times 10^{14}$ s^{-1}) carries 2.7×10^{-19} joules of energy.

A photon has no rest mass. However, based on Einstein's well-known formula, $E = mc^2$, where c ($= 2.9979 \times 10^8$ m s^{-1}) is the speed of light, it does possess a moving mass (m: kg) of $h\nu/c^2$. Since h is a constant, a photon's energy ($h\nu$) can also be expressed by its frequency: $\nu = E/h$. Furthermore, wavelength (λ: m = 100 cm = 10^6 μm = 10^9 nm = 10^{10} Å), wavenumber ($\tilde{\nu}$: m^{-1} = 0.01 cm^{-1}), and wave frequency (ν: s^{-1}) of a traveling photon with a fixed speed of light are related: $c = \lambda\nu$ and $\tilde{\nu} = 1/\lambda$. Therefore, one can also express a photon's energy in terms of its wavenumber: $\tilde{\nu} = E/hc$. When one says a photon of energy 667 cm^{-1} or 15 μm what that really means is that the photon has energy of $667\ cm^{-1} \times 6.626 \times 10^{-34}\ J\ s \times 2.9979 \times 10^{10}\ cm\ s^{-1} = 1.3 \times 10^{-20}$ J.

A particle, or matter (such as a molecule or an electron), has both rest mass (kg) and energy (J). The quantum view of matter as advanced by Niels Bohr to Max Planck's quantum hypothesis is that it too can only exist at discrete energy levels. For example, a molecule can rotate and vibrate only at certain discrete rates of frequency. A particle makes a transition from one of its energy states (E_i) to another (E_j) by absorbing or emitting a photon that has energy ($h\nu_0$) identical to the energy difference ($E_j - E_i$) of those two states. Since both the particle and photon can only have discrete energy levels, it should be quite clear at this point that a transition is impossible if $E_j - E_i \neq h\nu_0$. Furthermore, the energy levels of all substances are determined intrinsically by their masses and the internal structure of more elemental particles (such as electronic or atomic configurations in an atom or molecule). Hence, the absorption and emission spectra of various substances can be used as fingerprints of the matter. We have gained almost all our knowledge of the physical and chemical structure of stars and other planets by analyzing the emission and absorption spectra collected either from ground telescopes or from spacecrafts.

The microscopic interactions between a particle and a photon or among particles are usually studied on a one-to-one basis. The natural phenomena we encounter in daily life can be considered ensemble averages (statistical means) of various interactions between individual particles and discrete photons (radiative transitions) or among the individual particles (non-radiative transitions). Based on the concept of discrete energy levels one may ask: How could we have all those photons whose energies happen to match the exact differences of discrete energy levels of those matters? The simple answer is: those photons may have been originally released by particles when they made transitions from the higher energy levels to the lower ones.

Constant interactions between matter and photons (such as absorption and emission) are the nature of the existing world. An energy difference (~ 667 cm^{-1} or ~ 15 μm) between two vibrational states of a carbon dioxide (CO_2) molecule in the atmosphere happens to match

that of many photons emitted from the Earth's surface. A photon has to undergo repeated absorption and emission with CO_2 molecules before it finally escapes to outer space (a probability of less than 0.001) carrying energy or heat with it. The increase of CO_2 in the Earth's atmosphere further reduces the escape probability of the photons to space and may cause global warming. The very thick CO_2 atmosphere of Venus makes it almost impossible for its photons (at 15 μm) to escape to space. This leads to a very high surface temperature (~750 K) for Venus. One may wonder that if there are hardly any photons escaping from Venus surface then how do we know and verify its surface temperature? The answer to this question rests on the fact that there are lots of photons at other wavelengths (such as microwaves with wavelengths of millimeters and centimeters) that can escape directly from the surface of Venus to outer space and provide us with information.

Even if the condition $E_j - E_i = h\nu_0$ holds, it does not necessarily mean that the transition between E_i and E_j is possible. For example, the increase or decrease of the rate of vibration for a molecule can only occur one step at a time between two neighboring energy levels. Whether a particular transition is possible or not is determined by detailed analytical and numerical calculations of quantum mechanics and spectroscopy theory. The results can be summarized into sets of selection rules for different types of transitions (rotational, vibrational, and electronic) with some exceptions. For more detailed descriptions of the physical nature of absorption and emission processes readers are referred to McCartney (1983), Houghton and Smith (1966), and Levine (1975).

3. Macroscopic Radiative Transfer Equation and Its Formal Solution

The basic radiation quantity is the monochromatic specific intensity or the monochromatic radiance, $L_\nu(\mathbf{r}, \mathbf{\Omega})$, which can be considered a macroscopic ensemble of a stream of photons in a unit solid angle $d\Omega$, passing a spatial point $\mathbf{r}$, traveling in direction $\mathbf{\Omega}$, with frequency ν and speed c. The definition of $L_\nu(\mathbf{r}, \mathbf{\Omega})$ is also reflected in its unit: J m^{-2} steradian^{-1} = W m^{-2} Sr^{-1} Hz^{-1}. The macroscopic radiative transfer equation (RTE) is a continuity equation that describes the energy conservation of the photon stream as it interacts with matter along the path:

$$\frac{\partial L_\nu}{\partial t} + c\frac{\partial L_\nu}{\partial s} = c(\text{source} - \text{sink}), \tag{2}$$

where t is time and s the distance along the slant path of the photon stream. For most applications, the first term, the local time derivative in (2), is negligible because of the assumption of statistical equilibrium. The standard macroscopic RTE describes a spatial variation of a photon stream for an infinitesimal element ds (Fig. 1):

$$\frac{dL_\nu(s,\mathbf{\Omega})}{ds} = -k_\nu \rho_a L_\nu(s,\mathbf{\Omega}) + k_\nu \rho_a J_\nu, \tag{3}$$

where ρ_a (kg m^{-3}) is the density of radiatively active gas, k_ν (cm^2 kg^{-1}) is the extinction coefficient that linearly parameterizes the "sink" term in (2), and the source function J_ν in the "source" term ($k_\nu \rho_a J_\nu$) describes the rate of increase of photon energy along the path. It is noted from (3) that the extinction of monochromatic radiance is linearly dependent on both ρ_a and L_ν. If we instead choose number density (n_a: m^{-3}) as our measure of the absorber amount in (3) then the extinction coefficient is referred to as a cross section (σ_ν: m^2) with $\sigma_\nu n_a = k_\nu \rho_a$. There are two physical processes, absorption and scattering, that remove photons from the photon stream along the path. In this article, we focus our quantitative discussion mainly on the absorption process in the middle atmosphere and planetary atmospheres.

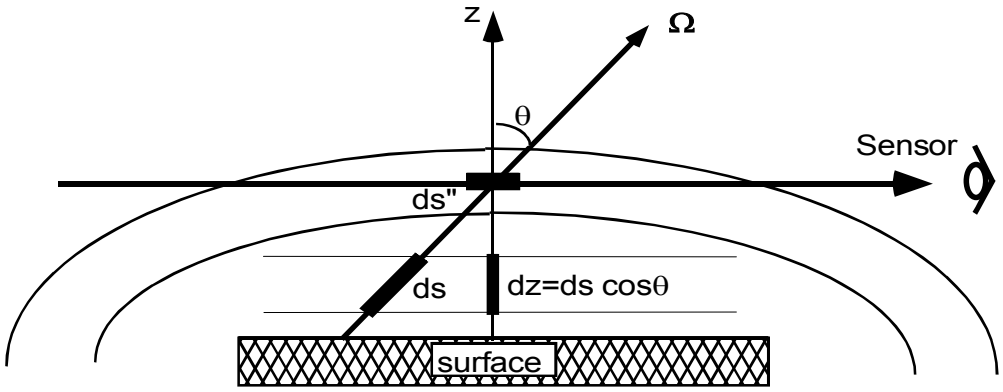

Figure 1. Infinitesimal element of a slant path (*ds*) and schematic illustration of limb (tangentially viewing) measurements of radiance.

Equation (3) can be easily integrated to yield the formal solution of monochromatic radiance,

$$L_\nu(s,\mathbf{\Omega}) = L_\nu(s_0,\mathbf{\Omega})\tau_\nu(s_0,s) + \int_{s_0}^{s}\left[k_\nu(s')\rho_a(s')J_\nu(s',\mathbf{\Omega};L_\nu)\right]\tau_\nu(s,s')ds', \tag{4}$$

where the *monochromatic transmission function,*

$$\tau_\nu(s,s') = \exp\left[-\left|\int_s^{s'} k_\nu(s'')\rho_a(s'')ds''\right|\right] \equiv \exp[-u_{\nu,\Omega}(s,s')], \tag{5}$$

is a basic building block in calculating any radiation quantity. The above solution also defines the *optical path* ($u_{\nu,\Omega}$) between s and s'. The solution (4) describes the fact that $L_\nu(s,\mathbf{\Omega})$ is composed of contributions from the boundary radiance $L_\nu(s_0,\mathbf{\Omega}) \equiv L_0$ exponentially attenuated by the optical path between s_0 and s plus the sum of the infinitesimal source function emission contributions from the internal atmospheric source term ($k_\nu \rho_a J_\nu ds' \equiv L_{atm}$) in the volume elements at positions s' along the path.

To illustrate the physical significance of the formal solution (4) and to also briefly review our knowledge of the interactions between radiation and matter described in the last section, let us consider two applications of (4) in retrievals of ozone (O_3) concentration (n_a) in the middle atmosphere. Depending on whether the largest contribution to $L_\nu(s, \mathbf{\Omega})$ in (4) comes from L_0 or from L_{atm}, the formal solution of (4) is the basis of two remote sounding techniques: occultation and emission-absorption (Fig. 1). The occultation technique neglects any contribution from L_{atm} and measures the ratio of the attenuated to the un-attenuated radiances, L_ν / L_0, from which the physical parameters, such as $\rho_a(s'')$, contained in $\tau_\nu(s_0, s)$ is derived. On the other hand, the emission-absorption technique measures the photons that are emitted within the atmosphere, L_{atm}, that have been attenuated by the rest of the atmosphere along the path as they reach to the sensor, $\tau_\nu(s, s')$. Both techniques are currently used for continuous measurements of O_3 profiles in the middle atmosphere by two different satellite instruments. The solar (or lunar) occultation technique employed by the Stratospheric Aerosol and Gas Experiment (SAGE, Chu and Veiga 1998) I, II, and III instruments, flown on several spacecraft platforms, uses the Sun (or Moon) as an external source (L_0) and uses the O_3 absorption feature in the ultraviolet (UV) wavelengths to provide the O_3 concentration. The limb emission-absorption technique employed by the Sounding of the Atmosphere using Broadband Emission Radiometry (SABER, Mlynczak 1997) instruments uses the infrared (IR) O_3 emission feature at the 9.6-μm band to continuously measure the photons along the whole satellite orbit. Since the Sun will get to the line-of-sight of the satellite sensor only twice (sunrise and sunset) in each orbit cycle, the spatial and temporal coverage of the occultation technique is usually very limited. Furthermore, nearly half of the section along the limb line-of-sight is in dayside whereas the rest is in nightside. The retrieval by the solar occultation is mathematically underdetermined if there exists a significant difference in O_3 concentration across the narrow twilight zone. Additional constraints are needed for a meaningful retrieval or interpretation in the retrieval algorithm. On the other hand, global coverage is much wider and more frequent when using the emission-absorption technique because the instrument is able to continuously collect photons along the whole satellite orbit. One disadvantage of the emission-absorption technique is that its measurements only provide indirect information about n_a. As an O_3 molecule in the atmosphere absorbs an UV photon in a Sun ray it makes a transition from its lower energy state (E_i: ground state) to an upper energy state (E_j). Therefore, the measured attenuation using the occultation technique $\tau_\nu(s_0, s)$ reflects the ozone population at its ground state (n_i). On the other hand, the photons collected by the emission-absorption technique represent the ozone population at its upper energy state (n_j: excited state) because the strength of the emission is nearly proportional to the relative population at its excited state (n_j / n_i). When $n_j << n_i$, the ozone population at its ground state as measured by the occultation technique can be considered the actual ozone concentration ($n_i \approx n_a$) whereas the emission-absorption technique relies on additional physical modeling that can accurately relate $n_j << n_i$ to n_a (e.g., Mlynczak and Drayson 1990).

Once the monochromatic radiance is known we can construct other radiation quantities that often involve integrating $L_\nu(s, \mathbf{\Omega})$ over a solid angle ($\mathbf{\Omega}$) to yield irradiance and over frequency (ν) to yield energy flux. A solid angle is determined by a zenith angle ($0 \le \theta < \pi$) and an azimuthal angle ($0 \le \varphi < 2\pi$). For middle atmospheric heating and cooling rate

calculations it is often a good approximation to assume a plane-parallel atmosphere (Fig. 1) and an isotropic source function:

$$ds = \frac{dz}{\cos\theta} \equiv \frac{dz}{\mu}, \quad J_\nu(s', \mathbf{\Omega}; L_\nu) = J_\nu(s'; \bar{L}_\nu), \tag{6a,b}$$

where $\bar{L}_\nu$ denotes the mean radiance averaged over the 4π solid angle (see Section 6). The basic building block between pressure levels p and p' can then be written as

$$\tau_\nu(p, p'; \mu) = \exp[-u_\nu(p, p') / \mu], \tag{7}$$

where the optical thickness between p and p' is

$$u_\nu(p, p') = \left| \int_p^{p'} k_\nu(p'')[r_a(p'')/g]dp'' \right|. \tag{8}$$

In (8), g (m s^{-2}) is the gravitational constant, and $r_a(p'') = \rho_a / \rho_{air}$ is the mass mixing ratio at pressure p'' with ρ_{air} defined as air density. We have also used the hydrostatic relation ($dp = -g\rho_{air}dz$) while converting (5) to (7). Note that the radiance is independent of φ except for the contribution from the boundary, which can be easily separated as shown in (4). The upward/downward energy flux (W m^{-2}) of the photon stream over a frequency band ($\Delta\nu$) can be calculated by

$$F^{\pm}(p) = 2\pi \int_{\Delta\nu} d\nu \int_0^{\pm\pi/2} \mu L_\nu(p, \mu) d\mu \,. \tag{9}$$

Note, from (9), that both F^+ and F^- are positive. The net energy flux is defined by the difference $F_n(p) = F^+(p) - F^-(p)$. Its convergence defines the radiative heating rate per unit mass (H_r: K s^{-1}) and is given by

$$H_r = \frac{-1}{c_p \rho_{air}} \frac{\partial F_n}{\partial z} = \frac{1}{c_p} \frac{\partial F_n}{\partial p}. \tag{10}$$

According to (4)-(9), calculations of energy flux and radiative heating rate involve multiple integrations over p, μ, and ν, respectively. Two basic quantities often used in the energy flux and radiative heating calculations that contain these multiple integrations are the flux transmission function (τ_f) and flux escape function (Γ_f) (Andrews et al. 1987) defined as

$$\tau_f(p, p') = \frac{2}{\Delta\nu} \int_{\Delta\nu} \int_0^1 \mu \exp\left[-\left| \int_p^{p'} k_\nu(p'')[r_a(p'')/g]dp'' \right| \Big/ \mu \right] d\mu d\nu \,, \tag{11}$$

$$\Gamma_f(p,p') = \frac{1}{S[T(p)]}\int_{\Delta\nu}\int_0^1 k_\nu[T(p)]\exp\left[-\left|\int_p^{p'} k_\nu(p'')[r_a(p'')/g]dp''\right|\Big/\mu\right]d\mu d\nu\,, \qquad (12)$$

respectively, where $S[T(p)]$ is the total band strength that is a function of temperature, T, at a given pressure level (p). We have also explicitly denoted that both the absorption coefficient k_ν and the mass mixing ratio of absorber r_a are functions of spatial position in terms of pressure.

The flux escape function $\Gamma_f(p, p')$ represents a radiative heat exchange of a frequency band ($\Delta\nu$) between p and p', which is the focus of this article. The net effect of such an exchange between one level and the rest of the atmosphere is the net radiative heating rate. By careful algebraic manipulations the radiative heating rate can be expressed as (e.g., Andrews et al. 1987, Zhu 1994)

$$H_r(p) = \frac{2\pi r_a(p)S[T(p)]}{c_p}\{-J_\nu(p)\Gamma_f(p,p_\infty) + [L_\nu(p_{00}) - J_\nu(p)]\Gamma_f(p,p_{00})$$
$$+\int_{\Gamma_f(p,p_\infty)}^1 [J_\nu(p') - J_\nu(p)]d\Gamma_f(p,p') + \int_{\Gamma_f(p,p_{00})}^1 [J_\nu(p') - J_\nu(p)]d\Gamma_f(p,p')\}\,. \qquad (13)$$

The four terms within the curly brackets in the above equation represent the radiative heat exchange between the photon energy at level p, $J_\nu(p)$, with (i) space ($L_\nu(p_\infty) = 0$); (ii) the lower boundary emission ($L_\nu(p_{00})$); and emissions from (iii) overlying and (iv) underlying layers, respectively. Equations similar to (13) can also be derived for the energy flux and flux transmission function. The fact that the heating rate is the vertical derivative of energy flux as defined in (10) is also reflected by the following relationship between τ_f and Γ_f,

$$\Gamma_f(p,p') = \frac{g\Delta\nu}{2r_a S[T(p)]}\left|\frac{\partial\tau_f(p,p')}{\partial p}\right|. \qquad (14)$$

Note that the crucial quantity $\Gamma_f(p,p')$ for the radiative heating or cooling rate calculation can be determined numerically either from its integral expression (12) or from the differential expression (14) once $\tau_f(p,p')$ is given.

Since the integrands in (11) and (12) are smoothly varying functions of p and μ, the integrations over p and μ are straightforward. Furthermore, the integrations over μ can be expressed in closed forms by exponential integrals (e.g., Abramowitz and Stegun 1965):

$$\tau_f(p,p') = \frac{2}{\Delta\nu}\int_{\Delta\nu} \mathrm{E}_3[u_\nu(p,p')]d\nu\,, \qquad (15)$$

$$\Gamma_f(p,p') = \frac{1}{S[T(p)]}\int_{\Delta\nu} k_\nu[T(p)]\,\mathrm{E}_2[u_\nu(p,p')]d\nu\,, \qquad (16)$$

where $\mathrm{E}_n(x) = \int_1^\infty t^{-n} e^{-xt} dt$ and $u_\nu(p, p')$ is as defined in (8). However, the integration over frequency poses a cumbersome problem in radiative transfer theory because the integrands that contain the absorption coefficient k_ν are composed of many lines and therefore are rapidly varying functions of ν. The traditional method of random band models explores the multiplication property of the exponential function $e^{x+y} = e^x e^y$ (see Section 5). Since neither exponential integrals nor the form of integrand in (12) possesses this property, i.e., $E_n(x+y) \neq E_n(x)E_n(y)$ and $(x+y)e^{x+y} \neq (xe^x)(ye^y)$, the random band models can only be applied to (11) by first integration over frequency, yielding the slant path transmission function. We will sketch the basic idea behind the traditional random band models and also present a recent approach of the correlated-k distribution method (CKD) in Section 5. But let us first briefly review some background on how line profiles are formed.

4. Quantum Concepts of Absorption/Emission Coefficients and Line Profiles

When the energy difference $(E_j - E_i)$ between two discrete states (n_j and n_i) is identical to that of a photon ($h\nu_0$), then there exists a possibility that the two will interact in various ways, for example:

Absorption:	$n_i + h\nu_0 \rightarrow n_j$,	(17a)
Emission:	$n_j \rightarrow n_i + h\nu_0$,	(17b)
Stimulated emission:	$n_j + h\nu_0 \rightarrow n_i + 2h\nu_0$,	(17c)
Scattering:	$n_i + h\nu_0 \rightarrow n_j^* \rightarrow n_i + h\nu_0$,	(17d)
Fluorescence:	$n_i + h\nu_0 \rightarrow n_j^* \rightarrow n_i' + h\nu'$,	(17e)

where n^*_j is the so-called "excited" state that can only exist for a very short time. In quantum mechanics, the energy dependence of particles (n_j versus n_i) is viewed as each excited state being a different particle. Hence, the above equations look just like chemical reaction equations in their appearance and contents. Note that the scattered photon on the right-hand-side of (17d) travels in a different direction from the incoming photon whereas the induced photon on the right-hand-side of (17c) travels in the same direction and with the phase as the incoming photon. In the case of fluorescence, both the state n'_i and the scattered photon energy $h\nu'$ could be different from the original ones of n_i and $h\nu_0$.

Up to this point, we have only presented the simple view that radiative transitions occur only when the photon energy coincides exactly with the difference between two transition states $E_j - E_i = h\nu_0$. This corresponds to a resonant interaction when both states in transition are assumed to be stationary, which correspond to pure sinusoidal waves with fixed amplitudes. To quantitatively illustrate such a transition and relate the process to a δ-function distribution in frequency space we note that quantum mechanics expresses the state of a system in the form of wave functions. The wave functions for states i and j of energies E_i and E_j can be expressed as ($\hbar = h/2\pi$)

$$\Psi_i \sim \exp(-iE_i t/\hbar)\,,\ \Psi_j \sim \exp(-iE_j t/\hbar)\,. \tag{18}$$

The intensity of a radiative transition (a_t) between states i and j is proportional to ($\omega_0 = 2\pi\nu_0$)

$$a_t = \Psi_i^* \Psi_j \sim \exp(-i(E_j - E_i)t/\hbar) = \exp(-i\omega_0 t)\,. \tag{19}$$

The photon distribution function in frequency ($f_\omega \sim f_\nu$) is proportional to $|a_\omega|^2$ from which we have

$$f_\omega = |a_\omega|^2 \sim \delta(\omega - \omega_0), \tag{20}$$

where $a_\omega = \int_{-\infty}^{\infty} a_t \exp(i\omega t)dt$ is the Fourier transform of a_t, and we have also normalized the frequency distribution function $\int_{-\infty}^{\infty} f_\omega d\omega = 1$.

Both laboratory measurements and more detailed theoretical analyses suggest that emission and absorption lines have finite widths due to several mechanisms. One mechanism that broadens the frequency distribution function is the finite lifetime of an emitting particle (atom or molecule) staying at a particular state. To illustrate this process, let us consider the effect of finite lifetime of the state j when a radiative transition from state j to state i occurs. The probability P_{decay} for an emitting particle to remain in its initial state j before making a transition by emitting a photon is $P_{decay}(t) \sim \exp(-t/\tau_d)$, where τ_d is the mean lifetime of the state j. Since an observed emission line represents an ensemble average of many photons with various lifetimes, the Fourier component of the transition intensity can be written as

$$\overline{a}_\omega = \int_0^\infty a_t \exp(i\omega t)\exp(-t/\tau_d)dt = \frac{1}{\tau_d^{-1} + i(\omega - \omega_0)}\,. \tag{21}$$

Substituting (21) into (20) yields the following normalized Lorentz line profile

$$f_\omega^L(\xi) = \left|\overline{a}_\omega\right|^2 \sim \frac{\alpha_L}{\pi}\frac{1}{{\alpha_L}^2 + (\omega - \omega_0)^2} = \frac{\alpha_L}{\pi}\frac{1}{{\alpha_L}^2 + \xi^2}\,, \tag{22}$$

where $\alpha_L = 1/\tau_d$ is the Lorentz half-width and $\xi = \omega - \omega_0$. Note that δ-function can be expressed in many different limiting forms, specifically (e.g., Arfken 1985),

$$\delta(y) = \frac{1}{\pi}\lim_{x\to 0}\frac{x}{x^2 + y^2}\,. \tag{23}$$

Therefore, the idealized line profile (20) is recovered, $\lim_{\alpha_L \to 0} f_\omega^L = \delta(\xi) = \delta(\omega - \omega_0)$, as $\alpha_L \to 0$ or $\tau_d \to \infty$, which corresponds to the case of a stationary state.

Another broadening mechanism arises from the Doppler effect of thermal motion of the emitting particles. A photon wave packet of frequency ω traveling at the speed of light c emitted by a moving particle with a velocity u ($<< c$) in the direction of propagation of the photon is perceived by a stationary observer as having the emission frequency ω_0 replaced by a Doppler-shifted frequency $\omega' = \omega_0(1 + u/c)$. Again, the bulk effect of many moving particles on an emission line can be derived by averaging the Doppler shifts to the profiles by all the emitting particles,

$$f_\omega^V(\xi) = \frac{\alpha_L}{\pi}\int_{-\infty}^{\infty}\frac{P_D(u)du}{{\alpha_L}^2 + (\xi - u\omega_0/c)^2}, \tag{24}$$

where $P_D(u)$ is the Maxwellian distribution of the thermal velocity,

$$P_D(u) = \left(\frac{m_p}{2\pi k_B T}\right)^{1/2}\exp\left(-\frac{m_p u^2}{2k_B T}\right). \tag{25}$$

In (25), m_P (kg) is the mass of an emitting particle, T (K) is the temperature, and k_B (= 1.38×10^{-23} J K^{-1}) is the Boltzmann constant. $f_\omega^V(\xi)$, defined in (24), includes both Lorentz and Doppler effects and is called the Voigt profile. Based on the above derivation, the Voigt profile includes statistical means over two physical processes that can be considered to be independent: radiative decay and the thermal motion of moving particles. That an individual wave packet can carry both properties and be averaged is similar to a case that a physical quantity (F) can be a function of x, y, z, and t over which one can perform averages over more than one variables.

Substituting (25) into (24) and changing the integral variable, we have

$$f_\omega^V(\xi) = \int_{-\infty}^{\infty}\frac{\alpha_L}{\pi^{3/2}\alpha_D}\frac{\exp\left(-\eta^2/{\alpha_D}^2\right)d\eta}{{\alpha_L}^2 + (\xi - \eta)^2}. \tag{26}$$

Letting $\alpha_L \to 0$ and applying (23) to (26), we obtain the pure Doppler line profile

$$f_\omega^D(\xi) = \left(\pi^{1/2}\alpha_D\right)^{-1}\exp\left[-\xi^2/{\alpha_D}^2\right], \tag{27}$$

where $\alpha_D = (\omega_0 / c)(2k_B T / m_p)^{1/2}$ and $(\ln 2)^{1/2}\alpha_D$ is the Doppler half-width. Equation (26) indicates that, mathematically, the Voigt line profile has been expressed as a convolution of the Doppler and Lorenz line profiles

$$f_\omega^V(\xi) = \int_{-\infty}^{\infty} f_\omega^D(\eta) f_\omega^L(\xi - \eta)d\eta. \tag{28}$$

According to the convolution theorem for a pair of functions related by an integral transform the convolution relation between $f_\omega^L(\xi)$ and $f_\omega^D(\xi)$ implies a product relation between their inverse-transformed functions in the *t*-variable (e.g., Arfken 1985)

$$f_t^V(t) = f_t^L(t) f_t^D(t), \tag{29}$$

where f_t^L and f_t^D are the inverse Fourier transforms of $f_\omega^L(\xi)$ and $f_\omega^D(\xi)$:

$$f_t^L(t) = (2\pi)^{-1} \exp\left(-\alpha_L |t| - i\omega_0 t\right), \; f_t^D(t) = (2\pi)^{-1} \exp[-(\alpha_D^2 t^2/4) - i\omega_0 t]. \tag{30}$$

Our derivation of the Voigt line profile (26) demonstrates a clear physical significance of $f_\omega^L(\xi)$, $f_\omega^D(\xi)$, and the convolution relation (28). Also, note that an approximation of a linear relationship between the Doppler-shifted frequency and the velocity has been used in the derivation. However, the physical significance of f_t^L and f_t^D in the product relation (29) in *t*-variable is not obvious at all. This is a common situation in a convolution-product relationship associated with an integral transform where only one side of the equation shows a clear physical significance. Two other examples in the field of radiative transfer are the frequency-dependent coefficients of phenomenological conductivity and permeability (Bohren and Huffman 1983, p. 15) and the multiplication property of the transmission function (Zhu 1995). In the first example, electric polarization and magnetization of the electromagnetic waves will be related to the electric and magnetic fields through convolution integrals of Fourier transforms. Only the frequency-dependent phenomenological coefficients that define product relations carry a clear physical meaning in this case. In the second example, the composite *k*-coefficient of a gas mixture can be related to those of individual gases through convolution integrals of Laplace transforms (Zhu 1995). The physical basis of such a convolution relationship is the multiplication property of the transmission function. Although only one side of the convolution relationship has a clear physical significance, the correct usage of its mathematical relationship will help avoid unnecessary confusions in applications (Goody et al. 1989, Zhu 1995).

5. Integration of Radiation Functions Over Frequency

The absorption coefficient k_ν is composed of all (N) the allowed transitions among different states with each transition having its line strength, s_i, and line profile, $f_\nu^i = f^i(\nu - \nu_i)$

$$k_\nu = \sum_{i=1}^{N} s_i f_\nu^i, \tag{31}$$

where we have substituted ω with $\nu = \omega/2\pi$. Since the line profile has been normalized, the total band strength over a frequency band that covers many lines is given by $S \equiv \int_{\Delta\nu} k_\nu d\nu = \sum_i s_i$.

Generally speaking, s_i is a function of temperature whereas f_ν^i depends on both temperature and pressure (e.g., McCartney 1983, Section 6.1). Fig. 2a (Section 5.2) shows a synthesized k_ν at three different pressures ($p_1 < p_2 < p_3$) and temperatures. From (27), we know that the Doppler half-width $\alpha_D \propto \sqrt{T}$. On the other hand, the collision-induced Lorentz half-width goes as $\alpha_L (= \tau_L^{-1}) \propto \rho_{air} \propto p$ because τ_L is proportional to the mean free path of particles, which is inversely proportional to ρ_{air}. Note that pressure varies by several orders of magnitude in the middle atmosphere whereas temperature usually varies by no more than a factor of 2. Therefore, differences in absorption/emission spectra among different levels in the Earth's middle atmosphere are mostly caused by the pressure variation.

One example that illustrates the strong effect of α_D on line profiles due to temperature variations is the hydrogen Lyman-α emission and absorption at 121.6 nm. The Lyman-α emission line from the Sun is the strongest line in the UV wavelengths, and it plays an important role in mesospheric O_3 photochemistry. A very high temperature in the solar hydrogen (H) atmosphere produces the emission line broadened by the Doppler shifting according to (27). On the other hand, the absorption by terrestrial H in the upper thermosphere has a narrower profile because of a much lower temperature than that of the Sun. As a result, the Lyman-α radiation reaching the lower thermosphere has a local minimum at its line center (e.g., Nicolet 1985).

Note from Fig. 2a, that k_ν rapidly varies with ν when the spectrum consists of many lines. Furthermore, a typical vibration-rotation band of a simple molecule, such as H_2O, CO_2, or O_3, will often consist of hundreds or thousands of significant lines. Therefore, a straightforward evaluation of integrals over frequency in (11) and (12), the so-called line-by-line (LBL) integration, is extremely time-consuming and impractical in many applications. Various techniques have been developed to efficiently and accurately approximate the integration over frequency (Goody and Yung 1989). In this section, we briefly review two such techniques: random band models and correlated-*k* distribution method.

5.1. *Classic Random Band Models*

The simplest situation for integrating (11) and (12) over frequency is the weak absorption for a homogeneous medium so that line overlapping can be neglected,

$$\bar{K} \equiv \frac{1}{\Delta\nu}\int_{\Delta\nu} K_\nu d\nu \equiv \frac{1}{\Delta\nu}\int_{\Delta\nu}\left[h_\nu \exp(-k_\nu m/\mu)\right]d\nu\,, \tag{32}$$

where $m = \left|\int_p^{p'}[r(p'')/g]dp''\right|$ is the absorber amount and $h_\nu = 1$ or $h_\nu = k_\nu$ for (11) or (12). The homogeneous assumption has been used in (32) when assuming k_ν is independent on the path (p''). Substituting (31) into (32) and making a few approximations, we obtain

$$\bar{K} = \frac{1}{\Delta\nu}\sum_{i=1}^{N}\int_{\nu_i-(\nu_i-\nu_{i-1})/2}^{\nu_i+(\nu_{i+1}-\nu_i)/2} h_\nu \exp(-k_\nu m/\mu)$$

$$\approx \frac{1}{\Delta\nu}\sum_{i=1}^{N}\int_{\nu_i-(\nu_i-\nu_{i-1})/2}^{\nu_i+(\nu_{i+1}-\nu_i)/2}\begin{pmatrix}1\\ s_i f_\nu^i\end{pmatrix}\exp(-s_i f_\nu^i m/\mu)d\nu$$

$$\approx \frac{1}{\Delta\nu}\sum_{i=1}^{N}\int_{-\infty}^{\infty}\begin{pmatrix}1\\ s_i f_\nu^i\end{pmatrix}\exp(-s_i f_\nu^i m/\mu)d\nu$$

$$= \frac{1}{\Delta\nu}\int_0^\infty p(s)ds\int_{-\infty}^{\infty}\begin{pmatrix}1\\ s f_\nu^i\end{pmatrix}\exp(-s f_\nu^i m/\mu)d\nu$$

$$= \frac{1}{\Delta\nu}\int_{-\infty}^{\infty}d\nu\int_0^\infty\begin{pmatrix}1\\ s f_\nu^i\end{pmatrix}\exp(-s f_\nu^i m/\mu)p(s)ds\,. \qquad (33)$$

The first line of the above expression replaces the integral over a narrow band ($\Delta\nu$) by a summation of integrals over sub-intervals containing individual spectral lines ($\int_{\Delta\nu}\rightarrow\sum_i\int_{\Delta\nu_i}$). The second line neglects contributions of line strengths from those outside the individual frequency interval, i.e., neglects the line overlap ($k_\nu \rightarrow s_i f_\nu^i$). The third line approximates the finite integrals by infinite ones in order to derive enclosed expressions for certain f_ν^i profiles ($\int_a^b\rightarrow\int_{-\infty}^{\infty}$). The fourth line replaces the summation over individual lines of different line strengths by an infinite integral with a line strength distribution function ($\sum_i X(s_i)\rightarrow\int_0^\infty p(s)X(s)ds$), where $p(s)$ represents the fractional numbers of lines with line strengths lying between s and $s + ds$. The last line exchanges the order of the two integrals since the integration over s can often be easily evaluated (e.g., Zhu 1989a).

The line strength distribution $p(s)$ is chosen in such a way that the double integral can be evaluated analytically so that $\bar{K}$ becomes an enclosed expression in terms of a few parameters. Those parameters describe the characters of line profile (e.g., $\bar{\alpha}_L$ and $\bar{\alpha}_D$) and the distribution function $p(s)$ (e.g., δ and β) (e.g., Zhu 1989a, Zhu et al. 1991)

$$\bar{K} = \bar{K}(\bar{\alpha}_L, \bar{\alpha}_D, \delta, \beta, ...)\,. \qquad (34)$$

Various analytic expressions of (34) have been derived for either a pure Lorentz profile or a pure Doppler profile (e.g., Goody 1952, Malkmus 1967, Zhu 1989a, 1990). To derive enclosed expressions for the most general Voigt profile one has to introduce piecewise approximations for the Voigt profile (Fels 1979, Zhu 1988). Here, it needs to be emphasized that we have assumed an homogeneous path while driving (33). Therefore, the optical thickness has been replaced by a product between a constant k_ν and the absorber amount along the path: $u_\nu = k_\nu m$. The mean Lorentz and Doppler half-widths along the path, $\bar{\alpha}_L$ and $\bar{\alpha}_D$, represent this approximation when the medium is inhomogeneous. Another important approximation used in deriving (33) is the neglect of the overlapping effect, i.e., that lines are well separated. This approximation usually holds only when the absorption is weak ($u_\nu/\mu << 1$). Finally, note that (33) applies to both the transmission and escape functions.

To include overlapping effects among the different absorption lines one has to use the multiplication property for the transmission function ($h_\nu = 1$ and $\bar{K} \equiv \bar{\tau}$); this is based on the assumption that the transmission functions of any two lines are uncorrelated

$$\bar{\tau}_{12} \equiv \frac{1}{\Delta\nu}\int_{\Delta\nu} \tau_{12} d\nu = \frac{1}{\Delta\nu}\int_{\Delta\nu} \exp[-(k_{\nu 1} + k_{\nu 2})m/\mu] d\nu = \bar{\tau}_1\bar{\tau}_2 + \overline{\tau'_{\nu 1}\tau'_{\nu 2}} \approx \bar{\tau}_1\bar{\tau}_2 , \tag{35}$$

where $k_{\nu 1} + k_{\nu 2} = s_1 f_\nu^1 + s_2 f_\nu^2$ is the composite absorption coefficient of line profiles, and ($\bar{\tau}_1$, $\bar{\tau}_2$) and ($\tau'_{\nu 1}$, $\tau'_{\nu 2}$) are the mean and perturbed transmission functions, respectively, e.g.,

$$\bar{\tau}_1 = \frac{1}{\Delta\nu}\int_{\Delta\nu} \exp(-k_{\nu 1} m/\mu) d\nu , \quad \tau'_{\nu 1} = \exp(-k_{\nu 1} m/\mu) - \bar{\tau}_1 \equiv \tau_{\nu 1} - \bar{\tau}_1 . \tag{36}$$

Note that the multiplication property strictly holds for the monochromatic transmission function ($\tau_{\nu 12} = \tau_{\nu 1}\tau_{\nu 2}$). It is also expected to be a good approximation for a narrow-band slant-path transmission function ($\bar{\tau}_{12} \approx \bar{\tau}_1\bar{\tau}_2$) when the lines are randomly distributed (Goody 1952, Goody and Yung 1989). However, one should expect the multiplication property to be a bad approximation for the flux transmission function of (11) ($\bar{\tau}_{f12} \neq \bar{\tau}_{f1}\bar{\tau}_{f2}$) since the exponential integral, $E_3(x)$, does not possess the multiplication property. In practice, applications of random band models are often associated with the introduction of a diffusivity factor, $\eta \equiv 1/\mu_0 \approx 1.66$, that approximates the integration with respect to μ in (11) by a mean value of μ_0. Most importantly, the one-term approximate flux transmission function still possesses the multiplication property that is crucial for the random band models to include the overlapping effect as shown below.

Now, let us extend the multiplication property to many lines and define the band transmission function (Goody and Yung 1989)

$$\tilde{\tau} = \prod_{i=1}^{N} \bar{\tau}_i = \prod_{i=1}^{N} (1 - \frac{W_i}{N\delta}) , \tag{37}$$

where $\delta = \Delta\nu / N$ is the mean spacing between two lines and W_i is the equivalent width of a single line that characterizes the absorption

$$W_i \equiv \int_{-\infty}^{\infty} [1 - \tau_{\nu i}] d\nu = \int_{-\infty}^{\infty} [1 - \exp(-s_i f_\nu^i m/\mu)] d\nu . \tag{38}$$

Eq. (37) can be rewritten as

$$\tilde{\tau} = \exp\{\ln \prod_{i=1}^{N} (1 - \frac{W_i}{N\delta})\} = \exp\{\frac{1}{N}\sum_{i=1}^{N} \ln(1 - \frac{W_i}{N\delta})^N\} . \tag{39}$$

Noting that $\lim_{N\to\infty}(1-W_i/N\delta)^N = \exp(-W_i/\delta)$, we finally get the band transmission function including the line overlapping effect

$$\tilde{\tau} \approx \exp\{\frac{-1}{N}\sum_{i=1}^{N}(W_i/\delta)\} = \exp\{\frac{-1}{\Delta\nu}\sum_{i=1}^{N}W_i\} = \exp(-\bar{A}). \tag{40}$$

In (40), $\bar{A}$ ($=1-\bar{K}$ for $h_\nu=1$) is the band absorption for weak absorption as defined in (32). On the other hand, $\tilde{\tau}$ is also related to the band absorption $\tilde{A}$ by $\tilde{\tau}=1-\tilde{A}$ when the overlapping effect is included. When $\bar{A}<<1$, which corresponds to a case of negligible overlapping effect, we recover the weak approximation (34) for the band transmission function: $\tilde{A}\approx\bar{A}$ or $\tilde{\tau}\approx\bar{\tau}=1-\bar{A}$.

5.2. *Correlated-k Distribution Method*

In the last decade or so, it has become clear that the correlated-*k* distribution (CKD) method is a powerful tool for calculating radiation functions in inhomogeneous atmospheres. The *k*-distribution and its relation to band models were first introduced into atmospheric applications by Arking and Grossman (1972). The classical description of CKD emphasized the frequency distribution function *f*(*k*) (Domoto 1974). Shi (1981) suggested that the integration over frequency could be greatly accelerated by sorting an absorption spectrum into a monotonic function. Lacis and Oinas (1991) applied the *k*-distribution to radiative transfer problems in a vertically inhomogeneous atmosphere, formally defined CKD, and, more importantly, established a close connection between the cumulative frequency distribution, *g*(*k*), and the sorted absorption spectrum. West et al. (1990) suggested dispensing with *f*(*k*) and only considering the cumulative distribution function *g*(*k*) in radiation calculations. Although one needs *f*(*k*) to efficiently derive *g*(*k*), in numerical calculations the physical insights of radiative transfer in an inhomogeneous atmosphere can be mostly gained by only considering *g*(*k*). By introducing a perfect random band model in analyses, Zhu (1994) established a universal relationship among the exact LBL integration, CKD, and traditional random band models.

The *k*-distribution can be introduced from two different perspectives. One is to consider the *k*-distribution as a generalization of the traditional exponential-sum-fitting method where the slant-path transmission function for a homogeneous path can be expressed as (e.g., Wiscombe and Evans 1977)

$$\tau(m) = \sum_i a_i \exp(-k_i m) = \int_0^\infty f(k)\exp(-km)dk \equiv \mathcal{L}\{f(k)\}, \tag{41}$$

where $L\{\ \}$ denotes the Laplace transform. In (41), the first equality can be considered a discretization of frequency integration whereas the second equality applies the same tactic as the fourth line in (33) to *k*. Based on the second equality, $f(k)dk$ ($\approx a_i$) is the fraction of the frequency domain occupied by the absorption coefficient between *k* and $k+dk$. The second perspective of the *k*-distribution method is to first map the absorption coefficient k_ν in

frequency ν into a monotonic function k_g in a normalized variable $g \in (0, 1)$. Then, the integration over any radiation function such as (15) or (16) can be carried out with respect to g,

$$\frac{1}{\Delta\nu}\int_{\Delta\nu} R(k_\nu, m, ...)d\nu = \int_0^1 R(k_g, m, ...)dg \,. \tag{42}$$

Since k_ν, as defined by (31), is a rapidly varying function of ν, whereas k_g is a monotonic function of g expected to slowly vary, the right-hand-side of (42) can be evaluated far more efficiently than the left-hand-side.

The connection between the two perspectives can be established by introducing the cumulative distribution

$$g(k) = \int_0^k f(k')dk' \,. \tag{43}$$

Note that $dg = f(k)dk$. Furthermore, $g(k)$ is monotonic with $g(\infty) = 1$, i.e., the fraction of frequency that includes all values of the absorption coefficient is unity. From (41) and (42) we conclude that the integral variable g in (42) is the cumulative distribution function defined in (43). Based on the (41) and (43) we have

$$f(k) = \mathcal{L}^{-1}\{\tau(m)\}\,,\ g(k) = \mathcal{L}^{-1}\{\tau(m)/m\}\,. \tag{44}$$

The Laplace transform relationship between $\tau(m)$ and $f(k)$ (or $g(k)$) as indicated by (41) and (44) implies a convolution relation in $f(k)$ (or $g(k)$) when the multiplication property of $\tau(m)$ holds (Zhu 1995). The convolution formulas can then be used to derive the composite k-distributions for a gas mixture when the k-distributions for the individual gases are known.

Equation (41) suggests a one-to-one correspondence between the transmission function, $\tau(m)$, and the k-distribution, say, $f(k)$. However, $\tau(m)$ and $f(k)$ are completely different in terms of how they can be used to calculate other radiation quantities. The traditional $\tau(m)$ is an integral quantity that depends on the absorber amount (m) along the path. On the other hand, the k-distribution, $f(k)$, or k_g, is a localized quantity. In other words, even though the k-distribution as introduced by (41) and (42) has assumed a homogeneous path the derived $f(k)$ or k_g can be considered a parameter that may vary along the path. This crucial property of the k-distribution, first pointed out explicitly by Zhu (1995), is the reason that the k-distribution defined by (42) can be used to calculate any radiation function including those that have multiple scattering processes. Radiative heat exchange usually involves inhomogeneous atmospheres where the emission and absorption occur at different altitudes with significantly different spectra (Fig. 2a). Lacis and Oinas (1991) were the first to relate the validity or the accuracy of (42) to the correlation of spectra among different levels of an inhomogeneous atmosphere. They found the errors to be small (~1%) for the calculations of cooling rates by H_2O, CO_2, and O_3, and suggested CKD. Similar results of about 1 to 2% error were also

obtained while applying CKD to calculating other radiation quantities and with other gases (e.g., Fu and Liou 1992).

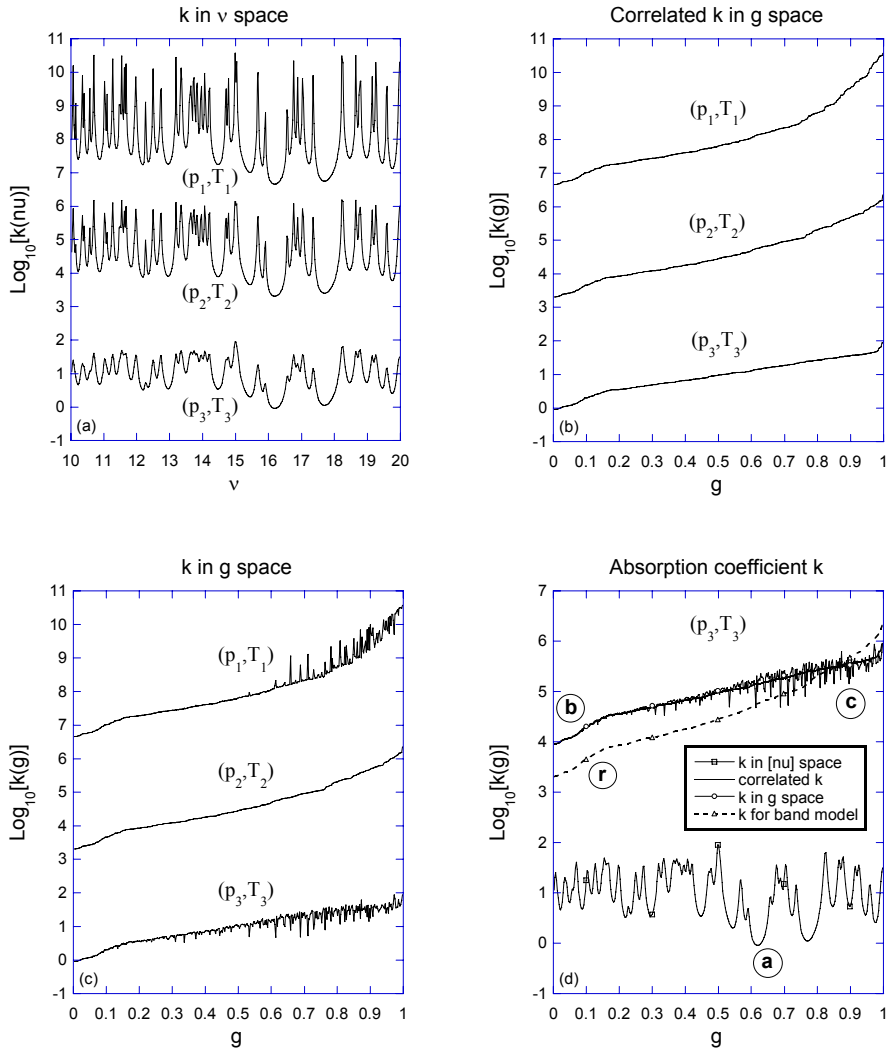

Figure 2. (a) Three absorption spectra in frequency variable synthesized from 60 Voigt lines with random positions and line strengths. (b) CKD derived directly by mapping each of the absorption spectra in (a) to a monotonically increasing *k*-distribution in a normalized *g*-variable. (c) When the spectrum at level 2 is mapped to a monotonically increasing *k*-distribution, the spectra at levels 1 and 3 are sorted accordingly. (d) All the absorption coefficients defined in (a-c) plus a *k*-distribution for a perfect random band model (denoted by **r**) and for level 3. In panels (a-c) the coefficients at level 1 have been moved up 4 units and those at level 3 have been moved down 4 units. In panel (d), only the original absorption coefficient in frequency space has been moved down 4 units (adapted from Zhu 1994).

To illustrate the relation between the correlation spectra and the validity of the CKD method we first map the synthesized k_ν at level 2 of (p_2, T_2) into a monotonic k_g as shown in Figs. 2b and 2c. However, since the radiative heat exchange is a non-localized process, the

spectra at other altitudes should also be sorted accordingly when calculating the radiative heat exchange among those levels. Assuming that the absorption and emission among different levels are strictly correlated (e.g., the maximum k_ν's at levels 1 and 3 occur at the same ν where k_ν at level 2 reaches its maximum), we can map the rest of the spectra at levels 1 and 3 into monotonic k_g spectra as shown in Fig. 2b. Immediately, we find that the *c*-*k* coefficients are much smoother than the original absorption coefficients. As a result, the integration over frequency in radiation calculations is greatly simplified and computationally comparable to that of a random band model such as (34) or (40).

The assumption of strict correlation in spectra among different levels (i.e., CKD) means that the absorption coefficients in Fig. 2a having the same ν at different levels will have the same g when they are mapped to the g-variable. There are few cases where this condition is strictly satisfied (Goody et al. 1989, Fu and Liou 1992). In general, the spectra among different levels are not strictly correlated. In other words, if we sort the spectra in all the other levels according to a reference level at which the absorption coefficient is mapped to a monotonically increasing *k*-distribution, then the sorted spectra in those levels will not increase monotonically. Figure 2c shows the *k*-coefficients at levels 1 and 3 sorted according to the mapping at level 2. As a result of such a simultaneous mapping, the calculated radiation quantities among these 3 levels will be identical for absorption coefficients in either Fig. 2a or Fig. 2c. Clearly, the difference between Fig. 2b and Fig. 2c determines the validity and accuracy of CKD.

To provide a universal assessment of validity for CKD without going over countless real examples of specific atmospheric and spectral specifications let us compare CKD with the traditional random band models, as described in the previous section, that are still widely used. For a random band model with a given $\tau(m)$, Eq. (44) defines the corresponding *k*-distribution for the band model. With the introduction of additional free parameters in (34) there will always be certain areas such as line shapes (Zhu 1988), line intensity distributions (Zhu 1989a), or band parameters (Zhu 1991) that can undergo improvement in random band models. This means that with great effort the derived *k*-distribution from a band model at a reference pressure and temperature could be very close to the actual LBL integrated *k*-distribution. A *perfect random band model* is one for which the inverse Laplace transform of its $\tau(m)$ matches the exact *k*-distribution. However, $\tau(m)$ is a quantity integrated along a finite path. Applications of $\tau(m)$ to a nonhomogeneous atmosphere always involve the use of certain scaling approximations such as the Curtis-Godson approximation (Goody and Yung 1989) such that the nonhomogeneous atmosphere is scaled to a uniform one with an equivalent pressure and temperature, say, (p_2, T_2). In other words, a perfect random band model will have its *k*-distributions at all levels identical to that of its reference level (Zhu 1994). Since the *k*-distribution is a localized quantity, the spatial inhomogeneity along the path can be easily incorporated by letting *k*-distribution vary with the actual p and T along the path, as shown in Fig. 2b.

A comparison of CKD with the LBL integration and a perfect random band model is shown by placing all three absorption coefficients defined in Figs. 2a-c for level 3 in the same figure plus the *k*-coefficient for the perfect random band model as in Fig. 2d. The latter is the *k*-coefficient at reference level 2 and is denoted by (**r**) in Fig. 2d. First, we note that the sorted curve (**c**) varies more rapidly than the original spectrum (**a**). Therefore, if we do not use the

"correlated" assumption, then mapping spectra alone does not simplify the calculations of radiative heat exchange. The figure shows that the CKD shown by curve (**b**) can be considered a smoothed spectrum of the exact curve (**c**). The most important fact from Fig. 2d is the comparison between curves (**b**) and (**r**), which illustrates the improvement of the CKD over a perfect random band model in accuracy. Since the major advantage of using a random band model is its computational speed, our analyses here demonstrate the additional superiority of CKD to the random band model of accurately incorporating the inhomogeneous effects. In other words, CKD takes advantage of both the accuracy of LBL integration and the efficiency of random band models. CKD is always more accurate because there exists a noticeable difference between CKD and a perfect random band model as indicated in Fig. 2d by curves (**b**) and (**r**). CKD is also efficient because it needs only a few points in g to integrate any radiation quantity by (42) regardless of how complicated the spectra are in ν.

To summarize the merits of the CKD method in comparison to the traditional random band models, we first note that the accuracy of the CKD method for a specific spectrum can be easily improved by increasing the quadrature points in the g-variable. On the other hand, a perfect random band model is only an ideal case that can hardly be realized to an arbitrary spectrum. In other words, even the accuracy of the frequency integration of a radiation quantity along a homogeneous path can be more systematically improved by the CKD method. The second merit of the CKD method is its more accurate treatment of the atmospheric inhomogeneity. This includes the elimination of both the path-length weighted means of the band parameters (e.g., Curtis-Godson approximation) and the diffusivity factor (η). The third merit is that any radiation quantity, such as $\Gamma_f(p, p')$, can be computed directly based on its well-defined formula, such as (12), by the CKD method. The last two merits have clearly been established on the basis that the k-distribution is a localized quantity. Radiation algorithms can easily take all these merits while adopting the CKD method. For example, Lacis and Oinas (1991) showed noticeable errors in $\tau_f(p, p')$ when the one-point diffusivity approximation is used in (11) for the integration over μ. Therefore, algorithms adopting the CKD method while still using the 1.66-diffusivity approximation have not taken full advantage of the method.

6. Microscopic RTE and Source Function

Equipped with the powerful computational tools for doing integrations over frequency as described in the last section, we can easily evaluate the radiative heating rate (13) once the source function (J_ν) is given. Under thermodynamic equilibrium (TE), J_ν depends only on T and is given by the well-known *Planck function*, $B_\nu(T)$ (e.g., Goody and Yung 1989)

$$J_\nu = B_\nu(T) \equiv \frac{2h\nu^3}{c^2}[\exp(h\nu / k_B T) - 1]^{-1}. \tag{45}$$

The basic physics of (45) is that the emission depends only on the relative population of the excited state n_j / n_i. Furthermore, n_j / n_i depends only on a well-defined T in a system under TE

through thermal contact (i.e., through collision processes) with a very large heat reservoir. When other processes such as radiative heat exchange become important, J_ν will no longer be determined by (45) but by a more general rate equation that includes both collisional and radiation processes. To derive J_ν under the breakdown of TE let us first derive the microscopic RTE that relates J_ν in (3) to the detailed interactions between radiation and matter. Assume that the lower (i) and upper (j) states have number densities n_i and n_j, and the degeneracies g_i and g_j, respectively. There are three fundamental radiation processes responsible for the change of radiance: absorption, spontaneous emission, and induced emission; see (17a-c).

The first process is the direct absorption of radiation (17a) that leads to an upward transition from i to j. The rate at which this process occurs for radiation of radiance L_ν can be written in terms of the *Einstein coefficient* B_{ij} as $(n_i f_\nu)B_{ij}L_\nu(d\Omega/4\pi)$, where $(n_i f_\nu)$ is the number density in state i that can absorb radiation at frequencies on the range $(\nu,\ \nu+d\nu)$. Here, f_ν is the normalized line (or band) profile. In making the transition from i to j, particles absorb photons of energy $h\nu_0 = E_j - E_i$. Thus, the rate at which energy is removed from an incident beam of radiation is given by

$$k_\nu^* \rho_a L_\nu \equiv s_i^* f_\nu L_\nu = n_i B_{ij}(h\nu_0 / 4\pi) f_\nu L_\nu , \tag{46}$$

where $s_i^* f_\nu = k_\nu^* \rho_a$ denotes a macroscopic absorption coefficient per unit length, uncorrected for stimulated emission. For particles returning from j to i, the two processes of spontaneous and stimulated emissions (17b-c) are possible. The rates of energy emission are given by $n_j(A_{ji}h\nu_0/4\pi)f_\nu$ and $n_j(B_{ji}h\nu_0/4\pi)f_\nu L_\nu$, respectively, where A_{ji} and B_{ji} are the Einstein coefficients for the spontaneous and stimulated emissions (e.g., Goody and Yung 1989).

Applying the continuity equation (2) or (3) of the energy conservation microscopically to a photon stream, we can write the RTE in terms of the microscopic quantities:

$$\frac{dL_\nu}{ds} = [-n_i B_{ij} L_\nu + n_j (A_{ji} + B_{ji} L_\nu)](h\nu_0 / 4\pi) f_\nu , \tag{47}$$

or a form similar to (3) in terms of the source function (L_ν) and line strength (s_i):

$$\frac{dL_\nu}{ds} = -s_i f_\nu (L_\nu - J_\nu) , \tag{48}$$

where

$$J_\nu = \frac{n_j A_{ji}}{n_i B_{ij} - n_j B_{ji}},\ s_i = \frac{h\nu_0}{4\pi}\left(n_i B_{ij} - n_j B_{ji}\right). \tag{49}$$

Equation (47) indicates that the change of radiance depends on the number densities (n_i, $i = 0, 1, 2, \ldots$) of particles at different energy levels. Interactions between matter and radiation

(radiative transition processes) as indicated by (17a-c) will change the distribution of n_i at various energy levels. Furthermore, interactions among the particles will also change the number distributions at different energy levels. For example, the following forward and backward collisional reactions will change the number densities:

$$\text{De-excitation:} \qquad n_j + M \rightarrow n_i + M', \quad k_{ji} \tag{50a}$$

$$\text{Excitation:} \qquad n_i + M' \rightarrow n_j + M, \quad k_{ij} \tag{50b}$$

where k_{ji} and k_{ij} (m^{-3} s^{-1}) denote rate coefficients for the reactions.

Equation (50a) denotes that a particle (say, a CO_2 molecule of ~ 360 part per million in volume $= 3.6 \times 10^{-4}$ in the Earth's atmosphere) at state i collides with a background medium M (a "heat bath" or a heat reservoir; for instance, an air molecule energetically coupled with all the other air molecules) to give out a portion of energy $\Delta E = E_j - E_i$ and to transit into state j. Equation (50b) denotes a similar reaction for the collision except in the reverse direction in which the particle acquires a portion of energy ΔE from the background medium. Here, the background medium is so large that it can absorb or give out almost any amount of energy without changing its own physical state ($M' = M$).

Considering a system that consists of many particles (say, $3.6 \times 10^{-4} \times 2.687 \times 10^{19}$ molecules $cm^{-3} \times 1\ cm^3 \approx 10^{16}$ molecules of CO_2) that is in contact with a heat bath, we ask the question of how the probability P_k (say, $= \prod_{j=1}^{1e16} p_{j,k}$) of the kth quantum state of the system depends on the value of its energy E_k (say, $= \sum_{j=1}^{1e16} \varepsilon_{j,k}$). According to statistical mechanics (e.g., Pathria 1996), in a long enough time (depending on the collision frequency and the efficiency of the energy transfer per collision) the system will reach a state of TE with P_k given by the following canonical distribution

$$P_k = \frac{g_k \exp(-E_k / k_b T)}{\sum_k g_k \exp(-E_k / k_b T)} \equiv \frac{g_k \exp(-E_k / k_b T)}{Q}, \tag{51}$$

where g_k is the degeneracy of the kth state and the normalization factor Q is called the partition function. The above equation suggests that under TE the system will have a greater probability of staying at a lower energy state than at a higher energy one.

The word "thermodynamic" contains the following two implications about the state of equilibrium. First, the equilibrium is established under a fixed thermal temperature T (or one could also consider that (51) leads to the definition of temperature). Second, it is a dynamical (rather than static) balance. In other words, it is the continuing energy exchange through (50) that brings about a balanced probability distribution (51). Based on this argument, the collisional rate coefficients k_{ji} and k_{ij} are related through $k_{ji} n_i M = k_{ij} n_j M$, or

$$k_{ij} / k_{ji} = (n_j / n_i)_{\text{equil}} = (g_j / g_i) \exp(-\Delta E / k_b T), \tag{52}$$

where (51) has been used to derive the second relation.

TE also implies that the radiance is homogeneous ($dL_\nu / ds = 0$) and isotropic ($L_\nu = J_\nu = B_\nu$). From (47), we have

$$-n_i B_{ij} L_\nu + n_j (A_{ji} + B_{ji} L_\nu) = 0 , \tag{53}$$

or

$$L_\nu = \frac{(n_j / n_i) A_{ji}}{B_{ij} - (n_j / n_i) B_{ji}} = \frac{(A_{ji} / B_{ji})}{\frac{g_i B_{ij}}{g_j B_{ji}} \exp(h\nu_0 / k_b T) - 1} = B_\nu(T) . \tag{54}$$

Comparing (54) with (45), we obtain the relationships among different Einstein coefficients

$$A_{ji} = (2h\nu_0^3 / c^2) B_{ji} , \quad g_i B_{ij} = g_j B_{ji} . \tag{55}$$

The absorption and emission coefficients are derived from the steady state measurements (and spectroscopy theory). However, microscopically, the absorption and emission coefficients are the intrinsic properties that describe the interactions between the photons and matter. This remains invariant even if the system deviates away from TE. The same idea also applies to the relation (52) between forward and backward collisional or chemical reaction rate coefficients k_{ji} and k_{ij} that have also been derived based on the assumption that the system is in TE. Microscopically, k_{ji} and k_{ij} are related to the intrinsic physical properties of those collisions among the particles and should be independent of whether the macro-system is in TE or not. Actually, our analysis on how the system arrives at TE through (50) has implicitly assumed that k_{ji} and k_{ij} would remain constant so that the system can reach a state of dynamical equilibrium.

Substituting (55) into (49) we finally relate the source function and the absorption coefficient to the particle populations n_j

$$J_\nu = \frac{2h\nu^3}{c^2} \left[\frac{g_j n_i}{g_i n_j} - 1 \right]^{-1} , \; s_j = A_{ji} \frac{c^2 n_i}{8\pi\nu^2} \frac{g_j}{g_i} \left[1 - \frac{g_i n_j}{g_j n_i} \right] \equiv s_j^* \left[1 - \frac{g_i n_j}{g_j n_i} \right] \tag{56}$$

subject to the constraint that the sum of n_i at all states gives the total number density of absorber: $\sum_i n_i = n_a$. In (56), s_j^* is the line strength without correction for stimulated emission. Laboratory measurements of absorption coefficients assume the TE condition and are given by

$$s_{TE} = s_i^* \left[1 - \exp(-h\nu_0 / k_b T) \right], \tag{57}$$

where we have applied (52) to the last identity in (56).

One still needs a set of equations that relate n_j to a known physical field or radiance to bring the system to a closure. In the most general approach, one has to again start from a conservation law of the particle stream similar to (2) that describes how n_i varies with time and space (e.g., Lifshitz and Pitaevskii 1981). The steady state solution (52) shows that n_i is solely determined by T under the TE condition. Equation (52) has been derived from the statistical physics that studies the special laws governing the behavior and properties of macroscopic systems. It reduces the total number of freedoms of the microscopic system (say, 10^{16} molecules) into a very small number of the corresponding macroscopic system (say, 2, T and p) as shown in (51) and (52). However, most useful results in statistical physics have been derived based on the fundamental premise that the (closed) system is under TE. This assumption eliminates both temporal and spatial changes.

To account for the temporal-spatial changes of a system while still preserving the key idea of macroscopic TE we review the concept of a continuum or fluid. Any small volume element in a fluid is always supposed to be large enough (greater than the mean free path of the particles) that it contains a great number of particles and photons. This assumption makes TE a very good approximation in the volume. In addition, the volume element is also relatively small so that its macro-physical properties can be considered a (slowly varying) continuous function of time and space. For example, instead of a fixed temperature T, we have the temperature of a fluid varying continuously with time and space: $T(t,x,y,z)$. Furthermore, the concept and the term "thermodynamic equilibrium" are expanded into "local thermodynamic equilibrium" (LTE) to reflect the fact that the canonical distribution (51) locally holds even though T is not a constant. The equilibrium n_j distribution at two energy levels (52) in a continuum becomes

$$[n_j(t,x,y,z)/n_i(t,x,y,z)]_{\text{equil}} = (g_j/g_i)\exp[-\Delta E/k_b T(t,x,y,z)] \tag{58}$$

and the corresponding LTE source function is given by (45). Specifically, if $n_i = n_0 \approx n_a$ ($\Delta E \approx E_j$) is the ground state, then (58) provides the relative populations of the excited states at various energy levels E_j ($j = 1, 2, 3, \ldots$).

To illustrate some implications of LTE, we note that (58) has been derived based on the collisional processes as to (50) by assuming a statistical equilibrium in a temporal-spatial domain over which an averaged T can be well defined according to (51). Since both relationships (51) and (58) depend on the energy levels, it is only natural to argue that whether a system can reach an equilibrium state through various collisional processes depends on ΔE ($\approx E_j$) and how efficiently the energy is exchanged among different particles through collisions. Hence, the concept of LTE or the definition of $T(t,x,y,z)$ based on (51) under LTE is also related to a specific frequency range ($\Delta E = h\nu_0$) over which the LTE relationship holds. From this perspective, the term "local" in LTE can also be understood as a portion of the whole energy or frequency coverage. The energies of different categories of electronic, vibrational, rotational, and translational transitions vary by many orders of magnitude. Furthermore, TE is attained by exchanging energy between the sub-system and a heat reservoir (through thermal contact, i.e., (50)). Therefore, a sub-system reaches LTE more

easily at a state corresponding to a translational or rotational transition with a smaller ΔE than at a vibrational or electronic transition with a greater ΔE.

LTE also depends on the size of the region over which one allows the collisional processes to occur to reach an equilibrium state. In the Earth's exosphere (z > 450 km), particles become near collisionless due to very low air densities (<5×10^7 cm^{-3}). A moving particle may easily escape to space or be subject to the influence of Earth's gravitational potential and travel in a ballistic orbit. As a result, the Maxwellian distribution (25) can no longer be used to describe the particles, kinetic energy that yields a well-defined translational T (e.g., Chamberlain and Hunten 1987, Strobel 2002) in the Earth's exosphere. On the other hand, many astronomical phenomena derived from ground-based observations can be explained by a well-defined (say, rotational) T (e.g., McKee et al. 1982) even when the particle densities in those objects (say, nebulae) are much lower (say, < 10^6 cm^{-3}). The implication of these two contrasting examples is that the measured nebula T has been averaged over a much greater volume in which particles experience collisions of many times to maintain an equilibrium distribution. In other words, the so-called intensive variables, such as n_i (= N_i / V) and T, are derived not by assuming the total number of particles at state i (N_i) and the volume (V) approaching to zero but by assuming that they are approaching infinity (e.g., Pathria 1996).

If additional processes such as radiative transitions and chemical reactions are needed and play non-negligible roles in terms of their magnitudes in order to derive n_i, then, we say that the system is in a state of non-LTE. The so-called rate equations illustrate the balance of populations when additional processes are included in considering a system in a statistical equilibrium. Here, we consider a radiative two-level model of the two vibration-rotation states j and i (e.g., Lopez-Puertas and Taylor 2001, Zhu 2003a)

$$n_j\left(A_{ji} + B_{ji}\bar{L}_\nu + k_{ji}[M]\right) + n_j D_j = n_i\left(B_{ij}\bar{L}_\nu + k_{ij}[M]\right) + \sum_\ell P_{\ell\to j} + P_{cj}, j = 1,2,3,\ldots \qquad (59)$$

where $k_{ji}n_jM$ and $k_{ij}n_iM$ represent the collisional processes (50), and $\bar{L}_\nu = (4\pi S)^{-1} \times \int_{\Delta\nu}\int_{4\pi} k_\nu L_\nu d\Omega d\nu$ is the mean radiance. The terms in the parentheses on both sides represent the rates of loss and production, respectively, for the state j. n_jD_j and $\sum_\ell P_{\ell\to j}$ denote the rates of loss and production, respectively, by collisional transitions other than (50) (Zhu 1990). The last term P_{cj} represents a net chemical production generated by photochemical reactions for the state j. Many applications of IR radiative transfer in the middle atmosphere and planetary atmospheres use the vibration-rotation spectra of gas molecules. In this case, it can be shown that non-LTE has little effect (< 5%) on s_i. On the other hand, J_ν can significantly deviate from its LTE value given by (45). Therefore, many non-LTE studies in the middle atmosphere and planetary atmospheres focus only on the non-LTE source functions. The rate equations (59) describe a localized statistical equilibrium at given states of molecules that correspond to certain energy levels. In principle, they are solved together with RTEs that relate the non-localized radiative energy exchanges among different layers of atmosphere to the changes of populations at those states.

It is also worth pointing out the difference between non-LTE and "not in TE." We note that neither the standard RTE (3) nor (59) contains any terms of time derivative in the closed

system. The non-LTE rate equations (59) still describe a state of dynamical balance between the production and the loss of the state population n_j except that additional physical processes have been added to TE. On the other, "not in TE" that refers to evolving L_ν or n_j often needs time-dependent continuity equations, such as (2), to describe the adjustment processes as the system deviates away from TE (e.g., Lifshitz and Pitaevskii 1981).

In general, the coupled equations are nonlinear and have to be solved through iteration (e.g., Zhu and Strobel 1990, Kutepov et al. 1998, Lopez-Puertas and Taylor 2001). One often requires calculations of broadband radiation quantities such as cooling rates or spectrally integrated limb radiances of radiatively active species (e.g., Goody and Yung 1989) for various modeling and retrieval applications. Under these circumstances, various approximations can be used to linearize the coupled equations to yield an enclosed expression for J_ν. Here, we briefly review and summarize a few approximations.

A vibration-rotation transition typically will have an energy difference ranging from 10^2 cm^{-1} to 10^4 cm^{-1}. In this case, n_j decreases rapidly with increasing j. The simplest non-LTE model is the classic two-level model that includes only the fundamental band ($0 \leftrightarrow 1$) corresponding to the transition between $j = 0$ and $j = 1$ (e.g., Houghton 1986). The non-LTE system is linearized and reduced into one rate equation and one RTE. Specifically, J_ν is the weighted average of the LTE blackbody source function B_ν and the mean radiance $\bar{L}_\nu$ whereas H_r is proportional to the difference between $\bar{L}_\nu$ and J_ν (Houghton 1986):

$$J_\nu = \frac{\phi_{10} B_\nu + \bar{L}_\nu}{\phi_{10} + 1}, \quad H_r = \frac{4\pi S r}{c_p} (\bar{L}_\nu - J_\nu), \tag{60}$$

where $\phi_{10} = k_{10} M / A_{10}$ is the ratio of collisional de-excitation to the Einstein coefficient. In the limit of LTE ($\phi_{10} \to \infty$) we have $J_\nu = B_\nu$ and $H_r \propto (\bar{L}_\nu - B_\nu)$. The latter relationship indicates a technical difficulty of evaluating H_r, for it usually involves a small difference between two large quantities. In the limit of strong non-LTE, when $\phi_{10} \to 0$, we have $J_\nu = \bar{L}_\nu$ and $H_r = 0$. This limit corresponds to an isotropic and conservative scattering. J_ν and H_r can further be expressed in closed matrix forms.

When the fundamental band becomes extremely thick in exchanging radiative heat (say, $\Gamma_f << 0.01$), contributions from the weak hot bands (say, $1 \leftrightarrow 2$ and $2 \leftrightarrow 3$) and minor isotope bands become comparable to or more important than those from the fundamental band. One has to consider a generally nonlinear multi-level model to derive accurate source functions for different sub-bands. A major source of the nonlinearity comes from the so-called vibration-vibration (V-V) transitions, such as ($j = 1$ and 2),

$$n_{j-1} + n_{j+1} \leftrightarrow n_j + n_j, \qquad k_{vvf}, k_{vvb} \tag{61}$$

where the forward and backward transition rates are given by the nonlinear terms $k_{vvf} n_{j-1} n_{j+1}$ and $k_{vvb} n_j n_j$, respectively (e.g., Zhu and Strobel 1990).

To reduce the generally nonlinear multi-level system into a linear two-level system Zhu (1990) and Zhu and Strobel (1990) explicitly developed and tested an equivalent two-level

model that neglects V-V transitions for the middle atmosphere broadband cooling rate calculations, with J_ν and H_r being similar to (60) for individual sub-bands. Since the broadband cooling rate of an equivalent two-level model using a broadband Curtis matrix is efficient and accurate, it has been used in some radiation algorithms for middle atmosphere models (e.g., Zhu 1994). An improvement that partially includes the V-V transitions by parameterizing J_ν as a linear combination of two limiting J_ν's with an adjustable parameter was also suggested in Zhu (1989b). In Zhu (2003a), the equivalent two-level model was further extended to include an additional source term of chemical production generated by photochemical reactions for the upper-level energy states of gas molecules. The closed expressions of J_ν and H_r are similar to those of the equivalent two-level model except that B_ν is modified by a factor $(1 + \phi_c)$, with ϕ_c $(= P_{cj} / k_{ij} n_i [M])$ characterizing the ratio of chemical production to collisional excitation.

7. Applications of Radiative Transfer to Planetary Atmospheres and the Earth's Middle Atmosphere

The last two sections described the frequency integration ($\int_{\Delta\nu} L_\nu(\mathbf{r},\mathbf{\Omega}) d\nu$) and the source function (J_ν) determination. These are two essential parts of the theory and applications of radiative transfer in a clear-sky atmosphere. One may look at the problems of radiative transfer in a scattering medium in a similar way where the integration over the solid angle ($\int_{\Delta\Omega} L_\nu(\mathbf{r},\mathbf{\Omega}) d\Omega$) becomes critical and cumbersome because of the rapidly varying phase function (e.g., Bohren and Huffman 1983, Liou 1980). Different techniques such as (33) and (42) can be considered different ways to sum up the contributions from individual building blocks. From this perspective, solutions to RTEs can be considered bookkeeping exercises because the RTE (3) and its solution (4), including more specific ones such as (13), are simple. Most importantly, as we have already pointed out that, the coupled system of (3) and (59) does not contain any time derivative terms even though the concept of continuum (i.e., fluid) was used while deriving those equations. Note that many interesting phenomena and difficult theories in fluid mechanics (e.g., waves, instabilities, solitons, chaos, etc.) are associated with the evolving nature of the system that corresponds to the existence of time derivative terms (e.g., Andrews et al. 1987, Craik 1985). From this perspective, the radiative transfer theory as described by the steady state system of (3) and (59) is often considered a technique or a tool to be used in a broader context of scientific researches. Such a view toward radiation theory naturally leads us to propose an empirical rule of "optimizing computational accuracy and efficiency" for solving specific radiation problems.

We have shown in Section 5 that the CKD method takes advantage of the accuracy of LBL integration and the efficiency of random band models. Therefore, the CKD method should be considered a starting point for calculating any radiation quantity. With such an empirical principle in mind, the author developed radiative heating and cooling modules for modeling the atmospheres of Pluto and Titan (Saturn's largest moon) where the radiative cooling by the methane (CH_4), ethane (C_2H_6), and acetylene (C_2H_2) vibration-rotation bands and the radiative heating by CH_4 and a haze layer were treated uniformly by the CKD method (Strobel et al. 1996, Zhu 2003b). Previously, a radiation module of cooling and heating rates

by sulfur dioxide (SO_2) with similar spectral complexities was developed for modeling Io's (Jupiter's closest moon discovered by Galileo) atmosphere in which several forms of random band models were adopted (Strobel et al. 1994). Although the analytical expressions such as (34) could be simple and fast, in some cases the evaluation of the mean parameters ($\bar{\alpha}_L, \bar{\alpha}_D, \delta, \beta, ...$) was generally computationally time-consuming for an inhomogeneous atmosphere. One possible advantage of using random models could be one's research heritage where the preexisting programs and experience may lead to savings in developing a new set of programs for different sets of spectral parameters and atmospheric conditions. However, the author also found that the CKD method could handle different specifications more easily than random band models since the *k*-coefficients can be derived by a general LBL integration whereas analytical expressions such as (34) exist only under certain special conditions.

Another significant advantage of using the CKD method, especially for cooling rate calculations, is to avoid calculating a small difference between two large quantities. We have already shown (Section 5.1) that only $\tilde{\tau}$ and $\tau_f(p,p')$ are available from random models for an overlapping band though the cooling calculations require $\Gamma_f(p,p')$ that is related to $\tau_f(p,p')$ by the derivative relationship (14). We also note from (15) and (16) that $\tau_f(p,p) = \Gamma_f(p,p) = 1$. It is common in many applications that $\Gamma_f(p,p') << 0.1$ when $|p - p'|$ only corresponds to a few layers of atmosphere in a model. This suggests that the computation of $\Gamma_f(p,p')$ based on (14) will involve a small difference between two nearly equal values of $\tau_f(p,p')$. As a result, the cooling rate calculation in the Earth's middle atmosphere by the CO_2 15-μm band often requires $\tau_f(p,p')$ to be accurate up to five significant digits. Since the *k*-coefficient is a localized quantity that can be used to compute any radiation function according to (42), we can derive $\Gamma_f(p,p')$ directly from its integral definition (16) to avoid finite differencing $\tau_f(p,p')$. In addition to the radiative heating and cooling rates, photolysis rate calculations in modeling the photochemistry of the middle atmosphere and planetary atmospheres sometimes also involve integrations over the frequency with complex spectra. Under these circumstances, the CKD method should also be considered a preference (e.g., Minschwaner and Siskind 1993, Zhu et al. 1999).

We listed several advantages for the CKD method for solving general radiative transfer problems regarding accurately and efficiently handling the radiative heat exchange among different layers. There exist also some special cases of radiation problems where techniques other than CKD may be better in terms of an overall optimization with respect to computational accuracy and speed. We have shown in Section 5 (Fig. 2) that the improvement of the CKD method over the random band models in terms of accuracy is its more accurate treatment of inhomogeneity when the radiative energy is exchanged among different layers with different spectra. In some applications of planetary atmospheres, we have only limited information regarding the bulk structure of an atmosphere. The bulk property will be determined by the integral quantity such as the absorption or transmission of a whole atmospheric layer. In this case, the random band model is a better approach due to its simplicity. Here, we show an application of retrieving Io's SO_2 atmosphere by the Malkmus model that corresponds to the specification of $\alpha_D = 0$ and $p(s) = s^{-1}e^{-s/\sigma}$ in (33) (Malkmus 1967, Zhu 1989a).

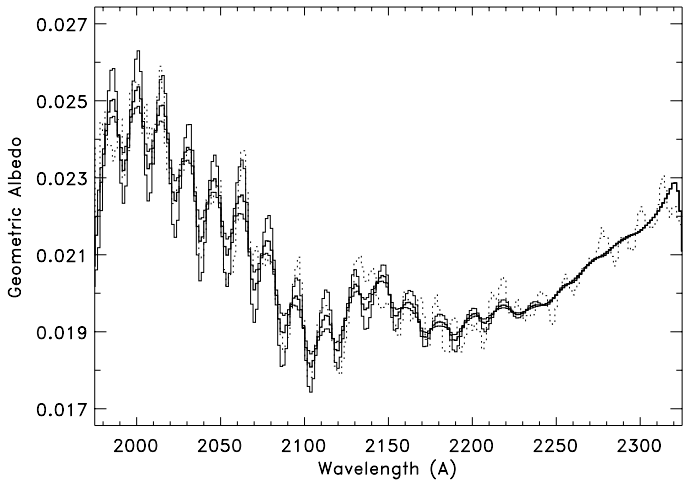

Figure 3. Measured and modeled geometric albedos over an SO_2 spectral region 1980-2300 Å for a hemispheric SO_2 atmosphere at 250 K. Short-dashed line: HST observed data; thick solid line: best fit by least-squares method with column density of 4.7×10^{15} cm^{-2}; thin solid lines: model albedos for the same atmosphere with the column density scaled up (down) by a factor of 2 that show greater (smaller) spectral contrast (after Ballester et al. 1994).

In Section 3 we described two techniques, occultation and limb emission-absorption, for atmospheric remote sounding. A third technique of analyzing the absorption-reflection spectra is illustrated in the retrieval of Io's SO_2 atmosphere and its physical properties. The solar photons reflected from Io were collected by a detector (Faint Object Spectrograph) on the Hubble Space Telescope (HST). The spectra of the reflected solar radiation depend on the atmospheric transmission and surface reflectance. Since gas and solid spectra are fundamentally different even for the same molecule (e.g., Houghton and Smith 1966), the spectral analyses of the so-called geometric albedo from Io provide us with information about the chemical composition and physical properties of Io's SO_2 atmosphere (Ballester et al. 1994). The geometric albedo is a function of the atmospheric transmission function ($\tilde{\tau}$) that is sensitive to SO_2 temperature (T) and its column density (N). Figure 3 shows one example of the measured and modeled Io geometric albedos over an SO_2 spectral region 1980-2300 Å for a hemispheric SO_2 atmosphere at 250 K and with $N = 4.7 \times 10^{15}$ cm^{-2}. In this case, we are not interested in details of photon exchanges within the atmosphere. The needed transmission function at each sub-band (i) for the whole atmosphere can be best derived by the simple Malkmus model (Ballester et al. 1994)

$$\tilde{\tau}_i(N) = \exp\left(-\frac{\pi y_i}{2} \left[\left(1 + \frac{4\sigma_i(T)}{\pi y_i} N \right)^{1/2} - 1 \right] \right) \quad \text{for each sub-band } \Delta\nu_i, \tag{62}$$

where the band parameters y_i and $\sigma_i(T)$ (i = 1, 2, …, 219) can be derived from laboratory measurements of high-resolution SO_2 spectra. A reasonably good fit between the measured and modeled geometric albedos, as shown in Fig. 3, justifies the inferred atmospheric T and

N. Recently, using the improved solar UV spectrum and a better database for the SO_2 spectrum, the differences in the measured and modeled geometric albedos with additional constraints have been further reduced (personal communications, K. L. Jessup).

Another special technique that is superior to the CKD method in terms of accuracy and efficiency is the table look-up method. When the physical property of the atmospheric state, such as $T(p)$ or mass mixing ratio $r_a(p)$, varies only slightly with respect to a reference state, the induced changes of the radiation quantities such as τ_f and Γ_f associated with the flux and cooling rate calculations are also expected to be small. In this case, the most efficient way to calculate the perturbed radiation quantity is the table look-up method. Chou and Arking (1978) first put forward such a radiation algorithm for the transmission function $\tau_f(p, p')$ to use in atmospheric numerical models. According to (11) and our discussions in Section 4, $\tau_f(p,p')$ is a functional of the atmospheric parameters of $T(p'')$, p'', and $r_a(p'')$ between levels p and p'. Chou's algorithm (Chou and Kouvaris 1991, Chou et al. 1995) stores the precomputed three-dimensional absorptance, A_{ijk}, as look-up tables

$$A_{ijk} = 1 - \tau_f(p^i_{eff}, w^j, T^k_{eff}), \quad i = 1, 2, \ldots, I; \quad j = 1, 2, \ldots, J; \quad k = 1, 2, \ldots, K, \tag{63}$$

where p_{eff} and T_{eff} are the effective pressure and temperature, respectively, averaged by the Curtis-Godson approximation, and w is the absorber amount between p and p'. Often, both p_{eff} and w vary by several orders of magnitude whereas T_{eff} varies no more than a factor of 2 in atmospheric models. For example, for the CO_2 15-μm band in the middle atmosphere, parameters I, J, and K can be set at 26, 21, and 3, respectively (Chou and Kouvaris 1991). Given $T(p'')$ and $r_a(p'')$ in a numerical model, $\tau_f(p, p')$ can be derived by interpolation formulas according to the stored A_{ijk} and the calculated (p_{eff}, w, T_{eff}) between p and p'.

Note that in addition to storing accurate tables A_{ijk} that can be derived by the LBL integration, the accuracy of Chou's interpolation algorithm also depends on the validity of the Curtis-Godson approximation. Fels and Schwarzkopf (1981) developed an interpolation algorithm that removed this limitation by a direct Taylor expansion of the transmission function between two model grids of p_j and p_k, $\tau_{jk} \equiv \tau_f(p_j, p_k)$ $(j, k = 1, 2, \ldots, N)$

$$\tau_{jk} \approx \tau^0_{jk} + \sum_{i=j}^{k} \frac{\partial \tau_{jk}}{\partial T^0_i}(T_i - T^0_i) + \sum_{i=j}^{k} \frac{\partial \tau_{jk}}{\partial r^0_{ai}}(r_{ai} - r^0_{ai}) \equiv \tau^0_{jk} + \sum_i B^0_{ijk}(\Delta T)_i + \sum_i D^0_{ijk}(\Delta r_a)_i, \tag{64}$$

where τ^0_{jk} is the transmission function calculated at the reference state of $T^0(p'')$ and $r^0_a(p'')$, and three-dimensional arrays $B^0_{ijk} \equiv \partial \tau_{jk} / \partial T^0_i$ and $D^0_{ijk} \equiv \partial \tau_{jk} / \partial r^0_{ai}$ are the stored coefficients used for the interpolation when the model $T(p'')$ and $r_a(p'')$ deviate from the reference ones. For the CO_2 15-μm band, $r_a(p'')$ is a constant in most numerical models. Hence, Fels and Schwarzkopf (1981) only considered the case $D^0_{ijk} = 0$. The size ($=N^3$) of the stored look-up table B^0_{ijk} that needs to be precomputed depends on the number (N) of model grids in vertical. Fels and Schwarzkopf (1981) factored the three-dimensional look-up table

into a two-dimensional one plus a vector that greatly saved off-line storage (= $N^2 + N$) and computational efforts for deriving the look-up tables

$$B^0_{ijk} = F_{jk} G_i , \quad (i,j,k = 1, 2, \ldots, N), \tag{65}$$

from which the interpolation algorithm for the CO_2 15-μm band becomes

$$\tau_{jk} \approx \tau^0_{jk} + F_{jk} \sum_i G_i (T_i - T^0_i) , \ (i, j, k = 1, 2, \ldots, N). \tag{66}$$

Most solutions to the radiative transfer problems in planetary atmospheres (as contrasted to stellar atmospheres in astrophysics) start with the transmission function, for instance, (63) and (64). One possible reason for this is that, historically, the most powerful tool of the random band models can only be developed for the transmission function, using the multiplication property to include the overlapping effect (Section 5.1). However, (15) and (16) suggest that there is little difference in computational efforts if the LBL integration or CKD method is used to perform the frequency integration over different radiation functions. Furthermore, heating or cooling rate calculations are better formulated by $\Gamma_f(p, p')$ than by $\tau_f(p, p')$, as shown in (13). Applying the similar idea of factoring to $\Gamma_f(p, p')$, Zhu (1990, 1994) developed a table look-up algorithm for calculating the middle atmosphere cooling rate by the CO_2 15-μm band and O_3 9.6-μm band

$$\Gamma_{jk} \approx \Gamma^0_{jk} + \alpha_j (T_j - T^0_j) + \beta_{jk} \sum_i G_i (T_i - T^0_i) + \gamma_j (r_{aj} - r^0_{aj}) + \delta_{jk} \sum_i G'_i (r_{ai} - r^0_{ai}) , \tag{67}$$

where Γ^0_{jk} is the flux escape function at the reference temperature (T^0_i) and mixing ratio (r^0_{ai}) profiles, β_{jk}, δ_{jk}, α_j, γ_j, G_i, and G'_i are the stored arrays and vectors all calculated off-line by the CKD method. Direct interpolation of (67) to obtain Γ_{jk} is intrinsically more accurate than that of (66) for the cooling rate calculations because it eliminates the unnecessary error introduced while taking the finite difference of τ_{jk} according to (14).

It is also interesting to make a comparison between Chou's algorithm based on the look-up tables (63) and those based on (66) and (67) from another perspective. Chou's algorithm has greater flexibility since the look-up tables are independent of individual models. On the other hand, the look-up tables in (66) and (67) are calculated based on the fixed model grids of p_k (k = 1, 2, …, N). However, the interpolations in (66) and (67) are explicit and straightforward whereas the multi-dimensional interpolation in Chou's algorithm requires the intermediate input of p_{eff} and T_{eff} that costs additional computational resources. This is one example illustrating a common trade-off between efficiency and flexibility one often encounters in the field of optimization. The so-called "No Free Lunch" theorems establish that an algorithm that is effective on one class of problems will always be offset by ineffectiveness on another class (Wolpert and Macready 1997). Therefore, selection of a particular algorithm or approach to a specific radiative transfer problem in planetary

atmospheres often involves considering an appropriate balance among accuracy, efficiency, and available resources.

The author's view of radiative transfer as a tool or a technique is based on the fact that given an input of atmospheric parameters (e.g., T and r_a) and a spectral database (e.g., Rothman et al. 1998), solution of the RTE (3) can be considered a well-defined and solved problem. The output could be various radiation quantities such as radiative energy flux or heating rate of the atmosphere. Note that the RTE (2) or (3) represents the basic law of energy conservation. Most science issues involving the Earth's middle atmosphere need to be resolved by incorporating additional conservation laws for momentum and mass, meaning that radiative transfer is coupled with dynamical, chemical, and transport processes in modeling and theories (e.g., Andrews et al. 1987, Brasseur and Solomon 1984, Zhu et al. 2000). This is mostly due to the advances in our acquired knowledge of the atmospheric state and the associated physical processes as a result of modern technology that provided us with tremendous amounts of measurements of both temporal and spatial coverage. Compared to the Earth's atmosphere, information derived from the observations of planetary atmospheres is still very limited. Often, the observed phenomena can only be investigated quantitatively by a particular conservation law, such as the RTE corresponding to the radiative energy conservation, even though processes associated with dynamics or other energy sources would certainly play roles. In this case, the solutions of the RTE associated with the energy conservation often involve specific science problems.

One application of using the RTE alone to solve a science problem is to determine and explain the vertical temperature profiles of planetary atmospheres. A good example of this type of work is the seminal paper by Hulburt (1931), who investigated the vertical temperature of the Earth's atmosphere based on limited observations and a clear-sky radiative transfer model. Using the measured absorbers and dividing the absorption spectrum into three sub-bands in solving the RTE, Hulburt (1931) was able to derive the vertical temperature profile of the Earth's atmosphere below 12 km that was consistent with the measured average temperature profile. We mentioned in the introduction that clouds play a major role in determining the energy budget in the troposphere. Even though the clouds were excluded in a clear-sky RTE, their effects were implicitly included in Hulburt's model for he assumed "… the incoming solar radiation of which 32 percent is reflected out to space by the surface of the earth and the clouds." Introducing an effective albedo to solar radiation while adopting a clear-sky RTE for cloudy atmospheres is an approximation often used even in modern research (e.g., Kasting 1988).

From the perspective of limited observations, the current studies of planetary atmospheres, especially the atmospheres of outer planets and their moons, are similar to that of the studies of the Earth's atmosphere in earlier history. Furthermore, our modern understanding of the problem allows us to make a retrospective assessment of earlier works. Therefore, it is worthwhile to list the following significant contributions and interesting points of the paper by Hulbert (1931):

- Specific absorbers and the measured absorption coefficients of H_2O and CO_2 were used. These are still the major absorbers in current modeling studies of Earth's atmosphere.
- A convective adjustment scheme was presented that redistributes the radiative energy in the vertical.
- Sensitivity studies of doubling and tripling CO_2 in the atmosphere were performed.
- Several feedback mechanisms among the surface temperature, H_2O, vegetation, snow covers, etc. associated with the CO_2-induced global warming were suggested.
- A major feature of an isothermal lower stratosphere above 12 km as observed at the time was not reproduced in the model since Hulburt (1931) did not include a UV spectrum in his model. This lack of reproducing observations without a correct mechanism makes the above-mentioned contributions even more valuable.

For the readers' convenience and entertainment, we show below three excerpts from Hulbert (1931) regarding the ideas of energy balance and convective adjustment, the doubling of CO_2 induced global warming, and the feedback mechanisms, respectively:

" If the convective region extended only to, say, 5 km we find that the atmosphere again is dynamically unstable and in addition that the total radiation emitted from the earth and the atmosphere is less than the energy received from the sun. When the convective region extends to 10 or 12 km (as is observed) the atmosphere is found to be stable, the calculated sea level temperature is about 290° (close to the observed value 287°) and the total radiation emitted from the earth and the atmosphere is equal to the received solar energy. If the convective region extended to a level greater than 12 or 15 km the outgoing radiation is less than the incoming solar radiation."

"Calculation shows that doubling or tripling the amount of the carbon dioxide of the atmosphere increases the average sea level temperature by about 4° and 7°K, respectively; halving or reducing to zero the carbon dioxide decreases the temperature by similar amounts."

"Further, an increase or decrease in the world-wide average atmospheric temperatures of a few degrees would give rise to other changes. The water vapor in the atmosphere would be increased or decreased, this would accentuate the temperature changes. At the same time changes in the areas covered by vegetation and snow fields would take place, thus changing the optical properties, that is, the emissive power *a*, section 5, of the surface of the earth."

Note that the 4°K increase in global mean surface temperature for doubling atmospheric CO_2 derived more than 70 years ago confirms to the current consensus derived by much more comprehensive three-dimensional general circulation models. However, the modern theory of global warming attributes major contributions to the feedback mechanisms (such as that due to water vapor) that were absent in Hulburt's model. Many physical numbers (not physical constants) undergo continuous revisions and fine tunings as new influencing factors, better measurements, and more efficient computational tools become available. It is often the fresh and fundamental ideas presented in original papers such the one by Hulburt (1931) that will last for a quite long time.

8. Concluding Remarks

In this article, the author presents a hierarchy of basic ideas and techniques of middle atmosphere radiative transfer. Though equations of various complexities are presented

throughout the article, the main focus is a step-by-step exposition of how to design a physically based algorithm for calculating any radiation quantity such as heating rates in planetary atmospheres. The establishment of RTE (2) or (3) is based on the energy conservation law. For clear-sky problems involving only absorption and emission processes, understanding of the spectral formation (Sections 2 and 4) and our two basic methods of integration over frequency (Section 5) will allow modelers to quickly design an effective algorithm for a specific problem. The rationales of several accurate and efficient approaches were explained through real examples, most of which the author had directly worked on (Section 7). A non-LTE parameterization for the source function (Section 6) often needs to be included in an algorithm for low-pressure conditions (say, < 0.1 mb = 10 pascal). The materials presented in this article have been mostly based on a part (~ 1.5 weeks) of a graduate course (Planetary Atmospheres) taught regularly by Darrell F. Strobel and the author at the Johns Hopkins University for the past decade. In this article, the author's expository review is limited to the theory of clear-sky radiative transfer. For more detailed theory and applications including the scattering, students are referred to other textbooks such as those by Houghton (1986), Andrews et al. (1987), Goody and Yung (1989), and Liou (1980). A modern textbook by Thomas and Stamnes (1999) that appropriately balances the depth and breadth of the field of radiative transfer has also been added to the reference list in recent years.

Acknowledgments. This research was supported by NASA grant NAG5-11962 and in part by NSF grant ATM-0091514 to The Johns Hopkins University Applied Physics Laboratory. The author thanks Dr. Elsayed Talaat for editorial assistance.

References:

Abramowitz, M. J. and I. A. Stegun, 1965: **Handbook of Mathematical Functions**. Dover, New York, 1046 pp.

Andrews, D. G., J. R. Holton, and C. B. Leovy, 1987: **Middle Atmosphere Dynamics.** Academic Press, New York, 489 pp.

Arfken, G., 1985: **Mathematical Methods for Physicists**. Third Edition. Academic Press, Inc., New York, 985 pp.

Arking, A. and K. Grossman, 1972: The influence of line shape and band structure on temperature in planetary atmospheres. *J. Atmos. Sci*., **29**, 937-949.

Ballester, G. E., M. A. McGrath, D. F. Strobel, X. Zhu, P. D. Feldman, and H. W. Moos, 1994: Detection of the SO_2 atmosphere on Io with the Hubble space telescope. *Icarus*, **111**, 2-17.

Bohren, C. F. and D. R. Huffman, 1983: **Absorption and Scattering of Light by Small Particles**. John Wiley & Sons, Inc., 530 pp.

Brasseur, G. and S. Solomon, 1984: **Aeronomy of the Middle Atmosphere: Chemistry and Physics of the Stratosphere and Mesosphere.** D. Reidel Publishing Company, Boston, 441 pp.

Chamberlain, J. W. and D. M. Hunten, 1987: **Theory of Planetary Atmospheres: An Introduction to Their Physics and Chemistry.** Second Edition. Academic Press, 481 pp.

Chou, M.-D. and A. Arking, 1978: An infrared radiation routine for use in numerical atmospheric models. Paper presented at *Third Conference on Atmospheric Radiation*, Am. Meteorol. Soc., Davis, Calif..

Chou, M.-D. and L. Kouvaris, 1991: Calculations of transmission functions in the infrared CO_2 and O_3 bands. *J. Geophys. Res.*, **96**(D5), 9003-9012.

Chou, M.-D., W. L. Ridgway, and M.-H Yan, 1995: Parameterizations for water vapor IR radiative transfer in both the middle and lower atmospheres. *J. Atmos. Sci*., **52**, 1160-1167.

Chu, W. P. and R. Veiga, 1998: SAGE III/ EOS, *SPIC*, **3501**, pp. 52-60.

Craik, A. D., 1985: **Wave Interactions and Fluid Flows.** Cambridge Univ. Press, Cambridge, 322 pp.

Domoto, G. A., 1974: Frequency integration for radiative transfer problems involving homogeneous non-gray gases: The inverse transmission function. *J. Quant. Spectrosc. Radiat. Transfer*, **14**, 935-942.

Emden, R., 1913: Uber Strahlungsgleichgewicht und atmospharische Strahlung. Ein Beitrag zur Theorie der oberen Inversion. Sitzungsberichte, Adademie der Wissenschaften, Munchen, No. 1, 55-142.

Fels, S. B., 1979: Simple strategies for inclusion of Voigt effects in infrared cooling rate calculations. *Appl. Opt*., **18**, 2634-2637.

Fels, S. B. and M. D. Schwarzkopf, 1981: An efficient, accurate algorithm for calculating CO_2 15 μm band cooling rates. *J. Geophys. Res*., **86**, 1205-1232.

Fu, Q. and K. N. Liou, 1992: On the correlated *k*-distribution method for radiative transfer in nonhomogeneous atmospheres. *J. Atmos. Sci.*, **49**, 2139-2156.

Goody, R. M., 1952: A statistical model for water-vapour absorption. *Quant. J. R. Meteorol. Roc.*, **78**, 165-169.

Goody, R. M. and Y. L. Yung, 1989: **Atmospheric Radiation: Theoretical Basis.** Second Edition. Oxford Univ. Press, New York and Oxford, 519 pp.

Goody, R., R. West, L. Chen, and D. Crisp, 1989: The correlated-*k* method for radiation calculations in nonhomogeneous atmospheres. *J. Quant. Spectrosc. Radiat. Transfer*, **42**, 539-550.

Houghton, J. T., 1986: **The Physics of Atmospheres.** Second Edition. Cambridge Univ. Press, New York, 271 pp.

Houghton, J. T. and S. D. Smith, 1966: **Infra-red Physics.** Oxford Univ. Press (Clarendon), London and New York, 319 pp.

Hulburt, E. O., 1931: The temperature of the lower atmosphere of the Earth. *Phys. Rev*., **38**, 1876-1890.

Kasting, J. F., 1988: Runaway and moist greenhouse atmospheres and the evolution of Earth and Venus. *Icarus*, **74**, 472-494.

Kibel', I. A., 1943: The temperature distribution in the Earth's atmosphere. *Dokl. Akad. Nauk SSSR*, **39** (1), 18-22 (in Russian).

Kutepov, A. A., O. A. Gusev, and V. P. Ogibalov, 1998: Solution of the non-LTE problem for molecular gas in planetary atmospheres: Superiority of accelerated lambda iteration. *J. Quant. Spectrosc. Radiat. Transfer*, **60**, 199-220.

Lacis, A. A. and V. Oinas, 1991: A description of the correlated *k* distribution method for modeling nongray gaseous absorption, thermal emission, and multiple scattering in vertically inhomogeneous atmospheres. *J. Geophys. Res*., **96**(D5), 9027-9063.

Levine, I. N., 1975: **Molecular Spectroscopy**. John Wiley & Sons, New York, 491 pp.

Lifshitz, E. M. and L. P. Pitaevskii, 1981: **Course of Theoretical Physics. Vol. 10: Physical Kinetics.** Butterworth-Heinenann, Oxford, 452 pp.

Liou, K. N., 1980: **An Introduction to Atmospheric Radiation.** Academic Press, New York, 392 pp.

Lopez-Puertas, M. and F. W. Taylor, 2001: **Non-LTE Radiative Transfer in the Atmosphere**. World Scientific Pub. Co., Singapore, 487 pp.

Malkmus, W., 1967: Random Lorentz band model with exponential-tailed S^{-1} line intensity distribution function. *J. Opt. Soc. Am*., **57**, 323-329.

McCartney, E. J., 1983: **Absorption and Emission by Atmospheric Gases: The Physical Processes**. John Wiley & Sons, New York, 320 pp.

McKee, C. F., J. W. V. Storey, D. M. Watson, and S. Green, 1982: Far-infrared rotational emission by carbon monoxide. *Astrophys*. *J*., **259**, 647-656.

Minschwaner, K. and D. E. Siskind, 1993: A new calculation of nitric oxide photolysis in the stratosphere, mesosphere, and lower thermosphere. *J. Geophys. Res*., **98**, 20,401-20,412.

Mlynczak, M. G., 1997: Energetics of the mesosphere and lower thermosphere and the SABER experiment. *Adv Space Res*., **20**(6), 1177-1183.

Mlynczak, M. G. and S. R. Drayson, 1990: Calculation of infrared limb emission by ozone in the terrestrial middle atmosphere. 1. Source function. *J. Geophys. Res.,* **95**(D10), 16,497-16,511.

Nicolet, M., 1985: Aeronomical aspects of mesospheric photodissociation: processes resulting from the solar H Lyman-alpha line. *Planet. Space Sci.*, **33**, 69-80.

Pathria, R. K., 1996: **Statistical Mechanics.** Second edition. Butterworth Heinemann, Oxford, 529 pp.

Pedlosky, J., 1987: **Geophysical Fluid Dynamics.** Second Edition. Springer-Verlag, New York, 710 pp.

Peixoto, J. P. and A. H. Oort, 1992: **Physics of Climate**. American Institute of Physics, New York, 520 pp.

Rothman, L. S. and collaborators, 1998: The HITRAN molecular spectroscopic database and HAWKS (HITRAN Atmospheric Workstation): 1996 edition. *J. Quant. Spectrosc. Radiat. Transfer,* **60**, 665-710.

Shi, G.-Y., 1981: An accurate calculation and representation of the infrared transmission function of the atmospheric constituents. *Ph. D. thesis*, Dept. of Science, Tohoku Univ. of Japan, 191 pp.

Strobel, D. F., 2002: Aeronomic systems on Planets, Moons, and Comets. in *Atmospheres in the Solar System: Comparative Aeronomy*, edited by M. Mendillo, A. Nagy, and J. H. Waite, pp. 7-22, AGU, Washington, DC.

Strobel, D. F., X. Zhu, and M. E. Summers, 1994: On the vertical thermal structure of Io's atmosphere. *Icarus*, **110**, 18-30.

Strobel, D. F., X. Zhu, M. E. Summers, and M. H. Stevens, 1996: On the vertical thermal structure of Pluto's atmosphere. *Icarus*, **120**, 266-289.

Thomas, G. E. and K. Stamnes, 1999: **Radiative Transfer in the Atmosphere and Ocean**. Cambridge Univ. Press, Cambridge, 517 pp.

West, R., D. Crisp and L. Chen, 1990: Mapping transformations for broadband atmospheric radiation calculations. *J. Quant. Spectrosc. Radiat. Transfer,* **43**, 191-199.

Wiscombe, W. J. and J. W. Evans, 1977: Exponential-sum fitting of radiative transmission functions. *J. Comp. Phys*., **24**, 416-444.

Wolpert, D. H. and Macready, W. G., 1997: No Free Lunch Theorems for optimization. *IEEE Trans. Evolutionary Computation*, **1**, 67-82.

Zhang, J., 1981: **Lecture Notes on Atmospheric General Circulation (in Chinese)**. Nanjing Institute of Meteorology Press, Nanjing, China, 313 pp.

Zhu, X., 1988: An improved Voigt line approximation for the calculations of equivalent width and transmission. *J. Quant. Spectros. Radiat. Transfer,* **39**, 421-427.

Zhu, X., 1989a: Radiative cooling calculated by random band models with $S^{-1-\beta}$ tailed distribution. *J. Atmos. Sci.,* **46**, 511-520.

Zhu, X., 1989b: A parameterization of cooling rate calculation under the non-LTE condition: Multi-level model. *Adv. Atmos. Sci.*, **6**, 403-413.

Zhu, X., 1990: Carbon dioxide 15-μm band cooling rates in the upper middle atmosphere calculated by Curtis matrix interpolation. *J. Atmos. Sci.,* **47**, 755-774.

Zhu, X., 1991: Spectral parameters in band models with distributed line intensity. *J. Quant. Spectrosc. Radiat. Transfer,* **45**, 33-46.

Zhu, X., 1994: An accurate and efficient radiation algorithm for middle atmosphere models. *J. Atmos. Sci*., **51**, 3593-3614.

Zhu, X., 1995: On overlapping absorption of a gas mixture. *Theor. Appl. Climatol.*, **52**, 135-142.

Zhu, X., 2003a: Parameterization of non-local thermodynamic equilibrium source function with chemical production by an equivalent two-level model. *J. Atmos. Sci*., submitted.

Zhu, X., 2003b: Examining the existence of superrotation in Titan's equatorial stratosphere: A paradigm for analyzing dynamical and thermal structures in slowly rotating planetary atmospheres. *In preparation*.

Zhu, X. and D. F. Strobel, 1990: On the role of vibration-vibration transitions in radiative cooling of the CO_2 15 μm band around the mesopause. *J. Geophys. Res.,* **95**(D4), 3571-3577.

Zhu, X., M. E. Summers, and D. F. Strobel, 1991: Analytic models for the ozone radiative absorption rate at 9.6 μm in the mesosphere. *J. Geophys. Res.,* **96**(D10), 18,551-18,559.

Zhu, X., J.-H. Yee, S. A. Lloyd, and D. F. Strobel, 1999: Numerical modeling of chemical-dynamical coupling in the upper stratosphere and mesosphere. *J. Geophys. Res.,* **104**(D19), 23,995-24,011.

Zhu, X., J.-H. Yee, and D. F. Strobel, 2000: Coupled models of photochemistry and dynamics in the mesosphere and lower thermosphere. in *Atmospheric Science Across the Stratopause*, edited by D. E. Siskind, M. E. Summers, and S. D. Eckermann, pp. 337-342, AGU, Washington, DC.